A MODEL SYSTEM FOR STUDYING BIOLOGICALLY COMPATIBLE COLLODIAL PROBES FOR CANCER RESEARCH

By
Samantha M Brandon

A thesis submitted to the Johns Hopkins University in conformity with the requirements for the degree of Masters of Science in Chemical & Biomolecular Engineering

Baltimore, Maryland
June 29, 2015

ABSTRACT

A Model System for Studying Biologically Compatible Colloidal Probes for Cancer Research

Samantha Mercedes Brandon, B.S., Johns Hopkins University

Co-Chairs of Advisory Committee: Dr. Michael A Bevan & Dr. Frechette

A key challenge in the development of targeted drug delivery techniques has been to further understand the weak, specific interactions between proteins and carbohydrates. The intermolecular forces between these biomolecules influence critical biological functions such as cell-cell adhesion, motility, signaling, proliferation, and metastasis. In the scope of cancer research, the CD44-Hyaluronic Acid (HA) complex is tightly coupled with many essential cellular functions and has been pointed to as a marker in cancer metastasis. While this complex has been studied thoroughly, there still lacks substantial measurements of the multivalent binding properties. This work attempts to fill that knowledge gap by utilizing lipid bilayers as a model cell system to study CD44-Hyaluronic Acid interactions.

In order to develop a controlled model of a cellular system, we utilized lipid bilayers integrated with a polymer cushion. With confocal microscopy, we were able to verify that the lipid bilayers formed planar monolayers on glass slides. Fluorescence Recovery After Photobleaching (FRAP) confirmed that the lipid bilayers maintained fluidity similar to that of *in vivo* cellular systems. We then determined the colloidal stability of the system by studying the interaction potentials of PEG (Polyethylene Glycol) coated and HA coated particles with the bilayer. These results demonstrate that the lipid bilayer system is suitable for studying CD44 interactions with HA modified particles.

Next, to study the multivalent interactions between CD44 and HA we integrated CD44 proteins into our lipid bilayer model. After isolating CD44 proteins from MDA-MB-231 breast cancer cells, we were able to integrate the transmembrane protein into our lipid bilayer. We confirmed this with confocal imagining and reassessed the stability of our system with PEG particles.

The specific binding of HA modified particles to CD44 was observed through TIRM. 100 kDa HA coated particles appear to formed clusters of stuck particles over regions of CD44 proteins, as was expected. This could indicate that not only is HA binding to CD44, but the CD44 proteins are also clustered together in lipid rafts. The robustness of this system was further demonstrated by inducing conditions that would inhibit HA-CD44 binding. The addition of 2mg/ml and 5mg/ml free 100 kDa HA to the bulk solution created competition of the HA binding domains. The TIRM data under these conditions resulted in potential energy profiles that show HA modified particles were stable above the lipid bilayer. Based on the findings in this work, a supported lipid bilayer based model cell system can be used to study the kT scale interactions of CD44 and HA.

To h&d, and k.

ACKNOWLEDGEMENTS

I would like to thank my friends and family for their love and support throughout this experience. My parents first and foremost for encouraging me to pursue this path. My dad for constantly encouraging me to follow what I truly love and inspires me. And my mom who is always a phone call away and full of practical advice, encouragement, or celebration when I needed it. My friends, who have always been the strong, independent people I can look to for support. Especially Jess, who made another year in Baltimore the best one yet. Kieran, for his patience and unyielding encouragement through all the ups and downs. And Duncan, for his brave endeavors into editing.

I would also like to thank all those within the academic community that have supported my work. My advisor, Dr. Bevan who first encouraged me to pursue my masters, has been a wonderful mentor throughout the whole process. My lab mates have been beyond helpful in teaching me new techniques and troubleshooting issues. Matt especially has given me invaluable guidance and advice at each stage. I would also like to thank those friends within the INBT who have helped me work through problems and given me new insights into my work. Finally, I would like to express my gratitude to all those that contributed in any small way to both my work and my person growth during this year.

TABLE OF CONTENTS

LIST OF FIGURES

FIGURE Page

LIST OF TABLES

TABLE Page

1. INTRODUCTION

1.1 Significance and Objectives

Understanding the intermolecular forces between proteins, carbohydrates, and other biomolecules has become increasingly important in understanding their role in cell behavior and medicine.[10,55] These weak, often specific interactions between proteins and carbohydrates influences critical biological functions such as cell-cell adhesion, migration, signaling, proliferation, and metastasis.[1-6] Understanding protein-carbohydrate interactions has also become a key challenge in the field of nanomedicine, especially for exploitation for the development of specific, targeted drug delivery techniques.[58]

Extensive studies have been done on the structure and function of a vast array of proteins and carbohydrates. Specifically, the transmembrane protein CD44 and its main binding target, Hyaluronic Acid (HA), have become a relevant interaction complex in cancer research.[59,60] CD44, a commonly expressed cell-surface glycoprotein, exists in many isoforms and is an important factor in cell adhesion, proliferation, migration, and other essential cell functions.[59,61] With its integral role in regulating many cellular functions, CD44 has been implicated in a number of diseases, especially cancer.[56,59-62] CD44's principal ligand, HA, has also been implicated for its inflammatory and tumorigenic responses.[61.65] HA is a ubiquitous glycosaminoglycan of the extra cellular matrix, and binds to the signal transducing CD44 receptors to play a major role in cell adhesion, motility, and proliferation.[64]

With more advanced tools such as the electron microscope and atomic force microscopy, we are able to visualize biomolecules on the nano scale and study the geometries of these individual molecules, especially bound structures.[37] Much work has been done to characterize structures of the CD44 isoforms, HA, and their bound complex.[37,59] From this work, studies have been done to understand the physical binding of these two molecules, and their relationship to cancer progression.[55-59] Insufficient measurement techniques limit further scientific exploration of the CD44-HA complex, impeding development of novel cancer treatments and targeted drug delivery. Current studies and measurements are unable to measure both the multivalent nature and microscopic affinity of binding, failing to describe CD44-HA's overall binding behavior.

To address this knowledge gap, our group has utilized Total Internal Reflection Microscopy to study protein and carbohydrate interactions on a biologically relevant scale.[29,39-41,50] In an effort to expand this work, we looked to combine various aspects of previous research on protein-carbohydrate interactions and lipid bilayer to develop a model system that can confirm previous findings and serve as a control for future work. Our focus here is to utilize CD44 proteins integrated into a lipid bilayer cell surface model to study interactions with HA coated colloidal probes. This work would confirm previous results and advance the use of HA coated colloidal probes in selective targeting and drug delivery.[31,50]

This work utilizes Brownian particles, also known as self-diffusing particles, which are controlled by potentials on the highly sensitive scale of thermal energy (kT). A well-established theoretical framework exists to explain the many important specific and non-specific interactions that occur in this range. These theories stand as the basis for this work, upon which we look to extend, develop, and refine methods of using self-diffusion colloidal probes to measure weak interactions between surface-immobilized biomolecules. The key results of this work are:

- An evaluation of non-specific interactions between PEG and Hyaluronic acid probes using total internal reflection microscopy
- The development a stable lipid bilayer that can be functionalized with proteins to represent a controlled model cell
- An evaluation of PEGylated lipid bilayer stability and interactions with PEG and Hyaluronic Acid probes using TIRM and video microscopy methods
- The isolation and examination of the CD44 protein from MDA-231 cells
- An examination of the CD44 functionalized lipid bilayers and their interactions with PEG and Hyaluronic Acid probes.

1.2 Background

The study of specific biomolecular interactions is limited by their measurement techniques, which can be divided into three mutually exclusive

categories: mechanical probes, spectroscopic techniques, and diffusing colloids. The most popular probe methods directly measure interactions (i.e., binding and bond rupture forces, dissociation constants) by externally manipulating the separation between opposing biomolecule-modified substrates. These measurements are based on the displacement of actual or effective springs, such as atomic force cantilevers or optical tweezers.[11-14] Spectroscopic techniques are also employed to make indirect, nonintrusive measurements. Interactions of soluble and surface-bound species can be quantified by measuring changes in interfacial, optical, or resonance signatures (e.g. fluorescence, refractive index, oscillation frequency).[15-18] While these measurement techniques provide insight into binding constants and rates and the net affinities of our system, they are ensemble averaged and do provide direct insight into our multivalent system of interest. To measure individual behaviors, we utilized a technique based on diffusing colloidal probe microscopy. The diffusion behavior of biomolecularly functionalized Brownian colloids can be observed using Total Internal Reflection Microscopy (TIRM). These observations can be interpreted using simple equilibrium statistical mechanics (i.e. Boltzmann distributions) to infer the relative energy of positions. This technique characterizes long range interactions, tethered chain mechanics, or binding lifetimes by passively measuring equilibrium positions of Brownian colloids proximal to neighboring surfaces, which also bear biomolecules.[19-22]

Each of the colloidal methods for studying biological interactions create a natural scale for measuring force (fN), time (a^2/D), length (nm), and energy (kT). Of the three techniques – mechanical probes, spectroscopic, diffusing colloids –

diffusing colloidal probes have been found to be the most sensitive in the investigation of biological interactions. The following sections will discuss basic concepts each of the three techniques as well as their advantages, disadvantages, and how they can complement each other.

1.2.1 Mechanical Probe Techniques

The development of scanning probe microscopy allowed for a new and more precise level of measurement. With the ability to measure interactions on the nanoscale, Atomic Force Microscopy (AFM) and Optical Tweezers (OT) are the two most widely used mechanical probe methods. These techniques employ the use of a probe near an interface and measures the probe-interface interactions by externally applying a force. Both of these methods have been used extensively to measure interactions between proteins, cells, and other biomolecules.[26,27] Specifically, AFM has been used to image the organization and determine binding strengths of the CD44-HA complex.[28,57] While both these tools are very useful, they are very limited in terms of sensitivity and do provide insight into the multivalent nature of our system.

1.2.2 Spectroscopy Techniques

Spectroscopic techniques allow for nonintrusive measurements that depend on the relationship between matter and electromagnetic radiation. The most common spectroscopic methods are Dynamic Light Scattering (DLS), Surface Plasmon Resonance (SPR), and Total Internal Reflection Fluorescence microscopy

(TIRFM). Each of these methods measures a response as a function of wavelength or frequency.

DLS is primary used to determine the size distribution of small particles in a known solution. Size is calculated by shining a monochromatic light beam through a sample to determine changes in the wavelength of light scattered by small particles. DLS is relevant in this work and in studying biological systems because it can relate size to the specific binding between proteins and colloids. DLS also facilitates investigation into the relationship between binding kinetics and solution chemistry, effective concentration, or particle surface chemistry.[30-31] DLS enables investigation of overall bulk solutions, but is unable to measure individual kT scale interactions.

Both SPR and TIRFM utilize evanescent waves from total internal reflection to measure binding equilibrium and kinetics. SPR measures changes at the interface of liquids and noble metals, while TIRFM measures changes in fluorescently labeled species. Both methods are useful for measuring average interactions in a variety of protein and cellular systems.[32-36] TIRFM is limited to only fluorescently labeled species, and both methods can only give results in average interaction potentials rather than individual interaction potentials.

1.2.3 Diffusing Probe Techniques

Passively tracking the diffusion of functionalized colloids has been found to be a highly sensitive, nonintrusive technique for probing weak interactions on the biologically relevant order of *kT*. Combining TIRM with video microscopy

enables us to study diffusing particles in 3D.[38] The evanescent wave generated by total internal reflection is scattered by the diffusing particles. The changes in intensity of this light scattering can be directly related to the height above the surface. A histogram of the sampled heights can then be translated into individual interaction potentials between particles and the surface. This technique, which can resolve 3D trajectories within ~1.5nm, has been a key tool in measuring interactions and binding lifetimes between non-specific biomacromolecules, specific proteins and carbohydrates, and lipid bilayers.[39-41] The sensitive nature of the evanescent wave scattering allows for very precise measurements, but in more complicated systems (i.e. live cells) additional scattering would add noise to the data.

1.2.4 Model Cell Systems

The study of specific biological interactions is also limited by the complex frameworks that comprise cellular systems. The wide array (proteins, membranes, vitamins, cells) of self-assembled cellular structures are governed by competing interactions, regulatory feedback loops, and branching pathways.[23] In an effort to understand complex biomolecular interactions, many studies have been conducted on isolated proteins, carbohydrates, etc. (using the aforementioned techniques). In order to further the development of novel, targeted sensing and drug delivery, CD44-HA and other metastatic interactions must be studied in models that mimic *in vivo* conditions.

Supported lipid bilayers (SLBs) have been found to possess the same 2D fluidity found in cell membranes, making them an ideal candidate for studying model cell systems.[66] They have been widely used to investigate membrane

structure, dynamics, and ligand-receptor binding.[29,67-69] Because CD44 is a transmembrane protein, we incorporate a polymer cushion into the bilayer to mitigate interactions with the substrate. This technique has been shown as a significant improvement to the bilayer model in that its 2D fluidity is consistently stable. This technique is even more representative of a cell model as the polymer cushion acts like a cytoskeleton of mammalian cell membranes.[70]

1.3 Summary and Outline

This dissertation is organized as follows: *Chapter 2* describes the theoretical aspects of (i) colloidal and surface forces and (ii) total internal reflection microscopy. *Chapter 3* outlines each experimental protocol in detail, including (i) materials and instruments, (ii) physisorption of pluronic, (ii) chemisorption of hyaluronic acid, (iii) lipid bilayer formation, (iv) cell culture, (v) immunoprecipitation, (vi) functionalization of lipid bilayers, and (vii) video microscopy and TIRM methods. *Chapters 4-6* detail experimental results from this work. *Chapter 4* sets the framework for developing a model lipid bilayer system by replicating previous results and measuring interactions between polymers and a lipid bilayer. *Chapter 5* presents a newly developed model cell system to study protein-carbohydrate interactions of CD44 and hyaluronic acid. This system is developed using functionalized lipid bilayers and characterized via TIRM. *Chapter 6* summarizes all final and overarching conclusion from this work. *Chapter 7* details multiple directions in which this work can be taken in the future.

2. THEORY

2.1 Colloidal and Surface Forces

The goal of this work is to study the forces of interaction between protein-carbohydrate and particle-cell systems. The separation-dependent interactions of these kinds of systems can be described independently from their geometry, so we are able to use simple colloidal particles against a flat wall to make these measurements using TIRM. The following describes the relevant equations to the surface and body forces governing our particle-wall system. This work focuses on the influence of gravitational, van der Waals, electrostatics and steric force contributions to these interactions, which are dominant in our systems of study. In order to evaluate the collective influence of these individual forces on the system, we assume a superposition of interaction energies. Therefore, the net particle-wall interaction can be explained as,

$$u_{pw}(h) = u_{grav}(h) + u_{VdW}h) + u_{electro}(h) + u_{steric}(h) \qquad (2.1)$$

where *h* is distance between the particle and its underlying surface, $u_{grav}(h)$ is the linear gravitational potential due to the weight of the particle, $u_{VdW}(h)$ is the potential due to long range van der Waals attraction, $u_{electro}(h)$ is contribution from electrostatic forces, and $u_{steric}(h)$ is the steric repulsion between opposing surfaces,. The net particle-particle potential is given by,

$$u_{pp}(r) = \sum u_{VdW}(r) + u_{electro}(r) + u_{steric}(r) \qquad (2.2)$$

where *r* is the separation between opposing particles, and the subscripts refer to van der Waals, and steric forces respectively. The overall interaction potential of the system is a summation of particle-particle and particle-wall interaction, given by

$$u_{net}(h,r) = u_{pw}(h) + u_{pp}(r) \tag{2.3}$$

2.1.1 Gravitational Interactions

The gravitational potential energy contribution is a body force that is the product of the height above the underlying wall, *h,* and the gravitational weight, *mg*. Its weight is dependent on densities of both the particle and the medium. The gravitational potential energy of each particle is dependent on its height above the wall, and is described by

$$u_{grav}(h) = mgh = \frac{4}{3}\pi a^3(\rho_p - \rho_f)gh \tag{2.4}$$

where ρ_p and ρ_f are the densities of the particle and medium, respectively.

2.1.2 van der Waals Interactions

Van der Waals forces arise from fluctuating polarizations due to dipole-dipole and dipole-induced dipole forces. These attractive forces and their associated screening, retardation, and geometric effects can be predicted in accordance with Lifshitz theory[42]. Lifshitz Theory incorporates materials properties with the Hamaker constant, $A_{132}(l)$, and represents the net van der Waals interactions as

$$u_{vdW}(h) = -\frac{a}{6}\int_h^\infty \frac{A_{132}(l)}{l^2}dl \tag{2.5}$$

where l is the distance between an individual particle and the wall. The Hamaker constant explains the interaction between materials 1 and 2, separated by a distance, l, within medium 3. For silica-water-silica van der Waals interactions, which are dominant in our system, we used

$$A_{132}(l) = \frac{2410}{a} kT^{1.195} \tag{2.6}$$

The Hamaker constant in our system is typically around 6nm. This impact of surface roughness can then be incorporated into the van der Waal interaction potential by approximating with an inverse power law fit to Liftshitz Theory. The van der Waals potential given as

$$u_{vdw}(h) = -aA_{132}(h + h_{wk})^p \tag{2.7}$$

where A is the effective Hamaker constant and p is a non-integer exponential. Both of these constants are the fitting parameters, and can be adjusted depending on the dielectric properties and geometry of the interaction components.

2.1.3 Electrostatic Interactions

Electrostatic interactions act as a stabilizing force to create colloidal stability. These repulsive forces arise from ionization, dissociation of surface charge groups, or adsorption of ions onto neutral surfaces. Without the presence of electrostatic repulsions, van der Waals attraction would cause particles to aggregate. In high salinity solutions (i.e. physiological strengths) long-range van der Waals forces dominate shorter-range electrostatic forces. The ionization of a

surface attracts high concentrations of salt from solution. The interaction of these opposing salt layers can be described as

$$u_{electro}(h) = B\exp(-\kappa h) \tag{2.8}$$

where B describes the materials properties and κ^{-1} is the Debye-length. In traditional systems, these forces act as a repulsive force between identical colloids and stabilize the system as a whole. However, at physiological strength the Debye-length is less than 1nm and electrostatic forces do not effectively create colloidal stability.

2.1.4 Steric Interactions

Nonspecific macromolecular interactions arise from the use of grafted or adsorbed polymer brushes on the surface of both wall and particle substrates. Under physiological conditions, these brushes will compress and provide a repulsive force that can provide colloidal stability at these conditions. The potential due to dense layer compression has been thoroughly studied and modeled by Milner et. al. as[45]

$$u_{steric}^{pw}(h) = \left(\frac{5}{9}\right)\frac{f_M}{k_BT}\left[\frac{1}{h/\Delta_0} + \left(\frac{h}{\Delta_0}\right)^2 - \frac{\left(h/\Delta_0\right)^5}{5}\right] \tag{2.9}$$

where Δ_0 is the uncompressed layer thickness and f_M is the free energy per unit area of the uncompressed brush. To account for changes in interactions due to geometry, the Derjaguin approximation can be used to calculate the overall steric potentials. This approximation can be further simplified using a short range exponential given by[39]

$$u_{steric}(h) = 16\pi a f_M \Delta_0 \left(\frac{\Gamma}{\gamma}\right) \exp(-\frac{h\gamma}{2\Delta_0}) \quad (2.10)$$

here, h is the compressed layer thickness of the symmetric brush layers. Γ and γ are dimensionless constants that are used to generalize equation 2.10 to other absorbed macromolecular architectures.

2.2 Total Internal Reflection Microscopy

Diffusing colloidal probes allows us to measure kT-scale energy wells by directly tracking an object's movement due to thermal energy. These measurements are a direct probe of the lowest energy states and weakest forces in an interaction system, making diffusing colloidal probes ideal for measuring weak, multivalent, and reversible interactions. Tracking of colloidal probes, with nanometer resolution relative to the wall, is most effectively done using TIRM. This technique utilizes the intensity of light scattered by a particle in an evanescent wave[6]. The intensity of scattered light is dependent on the instantaneous height of the particle, and can be related by

$$I_s(h) = I_0 \exp(-\beta h) \quad (2.11)$$

where I_s is the scattering intensity, I_0 is the intensity at height 0, and β is the evanescent decay length. This is calculated from

$$\beta = \frac{4\pi}{\lambda}[(n_1 \sin\theta_{inc})^2 - n_2^2]^{\frac{1}{2}} \quad (2.12)$$

where λ is the wavelength of the laser, n_1 and n_2 are the refractive indices of the incident and transmitted media, and θ_{inc} is the angle of incidence. This set up can be seen more clearly in Figure 2.1.

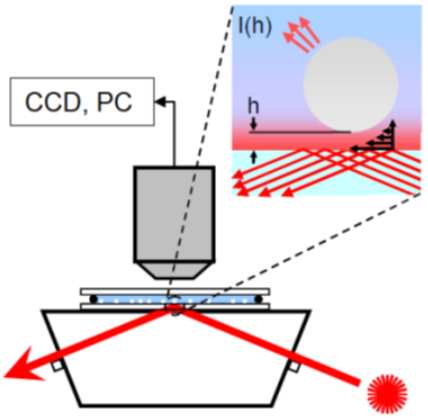

Figure 2.1: Schematic of a total internal reflection microscope, where the red lines represent the laser's light path[46].

Using image analysis algorithms coded in Fortran, we are able to use individual particle light scattering to track particles as they move in 3D[48]. The instantaneous heights of sampled particles can be can be plotted as functions of their intensity and time to render an intensity profile. The intensity profile can then be converted to a histogram of the most probable particle heights. Assuming a Boltzmann distribution, all final data can be translated into a potential energy profile that details the interaction between individual particles and the surface of the wall. The time-averaged height histogram can be related to the particle-wall potential with Boltzmann's equation, given as

$$p(h) = A \exp\left(-\frac{u(h)}{kT}\right) \tag{2.13}$$

3. EXPERIMENTAL METHODS

3.1 Materials

3.1.1 Generic Chemicals

Sodium chloride, hydrogen peroxide, sulfuric acid, phosphate buffer solution (PBS), magnesium sulfate, reagent grade chloroform, (3-aminopropyl)triethoxysilane (APTES), nitric acid, acetone, sodium azide, isopropanol, and toluene were all purchased from Sigma-Aldrich (St. Louis, MO) and used as received without further purification. All glassware was cleaned with Nochromix purchased from Godax Laboratories (Cabin John, MD). Colloidal probes in this work were coated in either PEO-PPO-PEO triblock copolymer Pluronic F108 purchased from BASF Corp (Wyandotte, MI) or 100 kDa Hyaluronic Acid purchased from Lifecore Biomedical (Chaska, MN).

3.1.2 Wall Surfaces and Particles

Nominal 2.34 μm silica microspheres (Bangs Laboratories, Fishers, IN) were utilized as colloidal probes throughout this work. Aluminum-free No. 2 22x22 VWR (Radnor, PA) selected micro cover glass slips served as the working surface for all experiments involving lipid bilayers. For all other experiments, Fisher Scientific (Pittsburgh, PA) glass microscope slides and Corning Life Science (Tewskbury, MA) cover slips were used.

3.1.3 Lipids

Lipid bilayers were comprised of 16:0-18:1 PC 1-palmitoyl-2-oleoyl-*sn*-glycero-3-phosphocholine (POPC) further stabilized with various concentrations of

1,2-diacyl-*sn*-glycero-3-phosphoethanolamine-N-[methoxy(polyethylene glycol)-2000] (mPEG 2000 PE), both purchased from Avanti Polar Lipids (Alabaster, AL). The bilayers were functionalized with 4-Di-16-ASP (4-(4-(Dihexadecylamino)styryl)-*N*-Methylpyriinium Iodide) (DiA) (LifeTechnologies, Grand Island, NY) to render fluorescent.

3.1.4 Antibodies and Proteins

Standard CD44s proteins were isolated from lysed cells by using the specific monocolonal anti-body Purified Mouse Anti-Human CD44 Clone 515 from BD Pharmingen (San Jose, CA). Once integrated into the lipid bilayer, CD44 activity was blocked by binding with the CD44/H-CAM Antibody (Hermes-1) (LifeTechnologies, Grand Island, NY). Isolation of the CD44 protein was characterized by first detecting concentrations using Micro BCA and the Micro BCA Protein Assay Kit (LifeTechnologies, Grand Island, NY). CD44 was specifically detected by running a Western Blot on NuPAGE Novex 3-8% Tris-Acetate Protein gels using the associated NuPAGE Tris-Acetate SDS buffer kit and NuPAGE Transfer buffer (LifeTechnologies, Grand Island, NY).

3.1.6 Cell Culture and Immunoprecipitation

MDA-MB-231 Human Breast Cancer Cells (Physical Sciences Oncology Center, Nation Institutes of Health, Bethesda, MD) were cultured in media comprised of Dulbecco's Modified Eagle's Medium (DMEM) with Penicillin-Streptomycin Solution (Sigma-Aldrich, St. Louis, MO). Cells were passaged on a regular basis by dissociating from flasks with Trypsin (Sigma-Aldrich, St. Louis,

MO) or gently with Enzyme Free Cell Dissociation Buffer, PBS (LifeTechnologies, Grand Island, NY). In order to isolated CD44 proteins, cells were lysed using a solution of Triton-X100, Nonidet P40 Substitute, Tris-Base, Tris-HCl, Ethylenediaminetretraacetic acid (EDTA), calcium chloride, sodium azide, and Protease Inhibitor Tablets (Sigma-Aldrich, Grand Island, NY).

3.1.7 Instruments

Colloidal probes were purified and washed using a MiniSpin-plus micro-centrifuge (Hamburg, Germany). Glass slides were functionalized with a silane linker using a spin coater (Laurell Technologies Corp, North Wales, PA). Protein electrophersis for Western Blotting was performed on a XCell SureLock Mini-cell (LifeTechnologies, Grand Island, NY). Western Blots were then imaged on a Bio-Rad Gel Doc XR+ System (Hercules, CA).

3.2 Methods

3.2.1 Physisorption of Pluronic

In order to mimic the conditions found *in vivo*, all experiments were carried out at physiological ionic strength – 150 mM NaCl. At this salt concentration, it is necessary to modify the surfaces of both the colloids and substrates to maintain interparticle stability and prevent adsorption of particles to the substrate. All colloidal particles utilized in this work were various micro- and nano- sized silicon dioxide; substrates were also composed on silicon dioxide. Colloids and substrates were first modified with a hydrophobic coating to allow for self-assembly of dense polymer or protein layers.

Glass microscope slides and cover slips were hydrophobically modified by spin coating polystyrene onto their surface. The substrates were first cleaned by sonication in acetone and isopropanol for 30 minutes, rinsed in DI water, and then placed in Nochromix overnight. Next, they were rinsed 10 times in DI water, sonicated in 0.1 M KOH for 30 minutes, and rinsed again 10 times. After drying under a stream of nitrogen, substrates were coated with a thin film of 3% (w/w) Polystyrene in toluene using a spin coater. A drop was placed at the center of the substrate and spun for one minute at 4,000 rpm.

Polymers were physisorbed to substrate surfaces in batch cells. After slides were allowed to dry for 30 minutes, batch cells were created by adhering a 1 mm Viton O-ring (McMaster Carr Inc, Robinsonville, NJ) onto the slide with vacuum grease. One hundred μL of 3000 PPM (3 mg/mL) solution of F108-Pluronic is added to the batch cell and allowed to adsorb overnight. The hydrophobic PPO chains of F108-Pluronic allow the polymer to form a monolayer on the polystyrene coated substrates, while the PEO chains extend away from the surface to form a brush layer. Excess, un-adsorbed F108-pluronic was removed by rinsing with phosphate buffered saline five times before each experiment.

Hydrophobically modified silica particles were obtained from a lab mate using a procedure adapted from literature that utilizes 1-octadecanol.[49] To adsorb the polymer to the 1-octadecanol coated silica particles, particles were dispersed in 3 mg/mL F108-Pluronic solution overnight. Excess F108-Pluronic is removed by centrifugation and re-suspension in DI water five times.

3.2.2 Chemisorption of Hyaluronic Acid

To study specific protein and polysaccharide interactions, colloids and substrates were functionalized with polysaccharide layers using a protocol adapted from literature.[50] The main polysaccharide of focus, Hyaluronic Acid (HA), is very hydrophobic and cannot physisorb to the previously hydrophobically modified colloids and substrates. In order to functionalize surfaces with the hydrophilic polysaccharide, silane chemistry was used to introduce functional groups that will chemically conjugate the polysaccharides to the surface. This method, as with the previous physisorption method, provides steric stability under physiological conditions.

Silica substrates were functionalized with Hyaluronic acid using an aminosilane linker to chemically graft HA.[50] Prior to functionalization, stock silica particles were washed five times by centrifugation in a micro-centrifuge and re-dispersion in fresh DI water. Particles were the re-dispersed in dry ethanol and washed an additional ten times in dry ethanol. To functionalize particles with an amino-silane, they were dispersed in a 2%(w/w) (3-aminopropyl)triethoxysilane (APTES) in dry ethanol. This particle solution was kept on a shaker for 24 hours. The reaction was stopped by washing the particles five times first in dry ethanol and then five more times in DI. Hyaluronic Acid solutions were made by dissolving 100kDa HA in DI water that was sterile filtered with an Anotop 0.02 μm syringe filter (Whatman, Pittsburgh, PA). HA could then be conjugated onto the surface by dispersing the particles in a sterile 10 mg/mL HA aqueous solution while being gently mixed with a magnetic stir bar. After 30 minutes, 2 Molar NaCl was added

to the solution to an overall concentration of 1 Molar. This gives the HA time to conjugate to the particle surfaces, and then allows for a denser HA layer by collapsing the long HA chains. After a total of two hours, excess HA was removed by centrifuge washing with DI and finally dispersed in PBS.

Glass slides were amino-silane functionalized in batch cells using a similar protocol. First, slides were cleaned as previously described with sonication in acetone and IPA for 30 minutes each, an overnight soak in Nochromix, and a 30 minutes soak in KOH. Cleaned and dried slides were placed in a 2% (w/w) APTES solution in ethanol for 20 hours. Excess APTES was removed by sonicating slides for 30 minutes in ethanol and then 30 more minutes in DI. After drying, batch cells were created by adhering a 1 mm O-ring onto the slide with vacuum grease. 60 μL of sterile 10 mg/mL HA was added to each slide, slides were kept in humidity. After 30 minutes, 60 μL of 2 Molar NaCl was added to each batch cell for an overall molarity of 1 Molar. One hour and 30 minutes later, for a total of two hours, batch cells were carefully pipette rinsed ten times with PBS.

3.2.3 Lipid Bilayer Formation

Supported Lipid Bilayers (SLBs) have been utilized as a successful model system for cell membranes for over three decades[51]. SLBs are an ideal model system to study cells and membrane proteins as they can be functionalized by ligands, undergo phase transitions, and possess transport properties similar to *in vivo* cell membranes. The SLBs utilized in this work were formed on a silicon dioxide substrate. Once formed, they are able to freely float on a 0.5-2nm thick layer of water, giving them a similar fluidity of freely suspended membranes.[3] In

this work, we increase the degree of separation between the bilayer and support by incorporating a polymer into the membrane.[52] As seen in Figure X, the polymer provides a low density hydrophilic brush layer above and below the bilayers. Incorporating a polymer into the SLBs is advantageous in that it reduces the friction between the bilayer constituents and the underlying support as well as reducing the non-specific binding of proteins to the support.[52] PEG was utilized throughout this work, providing our system with increased steric stability as well as tunability in terms of molecular weight and mole fraction of incorporated polymer.

We employed the extrusion method to prepare the small, unilamellar vesicles (SUVs) of uniform size that would form the final bilayer.[54,29] First, in a cleaned, chloroform rinsed glass vial, appropriate amounts of each lipid and/or polymer were mixed into a single solution. Chloroform was rapidly evaporated from this mixture under a stream of nitrogen, and then placed into a vacuum desiccator for at least five hours to ensure all the organic solvent has been removed. This dried lipid mixture was then reconstituted with 5mL of DI water for a concentration of 2mg of lipids/mL and dissolved completely by vortexing. At this point, the aqueous mixture is made up of multi-lamellar vesicles with a wide size distribution. The reconstituted aqueous mixture was then taken through 10 freeze-thaw steps using liquid nitrogen (-196°C) and a water bath heated to 80°C. The freeze-thaw cycles are critical to ensure proper fusion and rupture by breaking up the multi-lamellar vesicles.

Following the freeze-thaw cycles, the lipid solution contains highly polydispersed vesicles ranging in size from hundreds of nanometers to hundreds of

micrometers. Uniformly sized unilamellar vesicles were created by passing the solution ten times through a Lipex 10 mL extruder. The extruder held a track etch membrane and two membrane filters with an average pore size of 100nm. These filters were replaced following the first and fifth extrusion. Before use and each time filters were replaced, the extruder was thoroughly cleaned in DI water and EtOH. After extrusion, the average vesicle size was found using dynamic light scattering. Lipids were stored at 6°C and remained stable for up to two weeks.

The uniform unilamellar vesicles were formed into bilayers on Pirahna etched glass surfaces via vesicle fusion, rupture, and spreading. As show in Figure 3.2, deposited vesicles will first absorb to the surface due to nonspecific interactions. The vesicles will then begin to spread out along the surface, and once they reach a critical concentration, they will begin to fuse to their neighbors. This soon becomes two independent bilayers, where the top layer, having no attachment to the support, will reassemble into vesicles in the bulk solution.[29] The incorporated polymer will help facilitate diffusion of the bilayer over the support and fill in any gaps or defects.

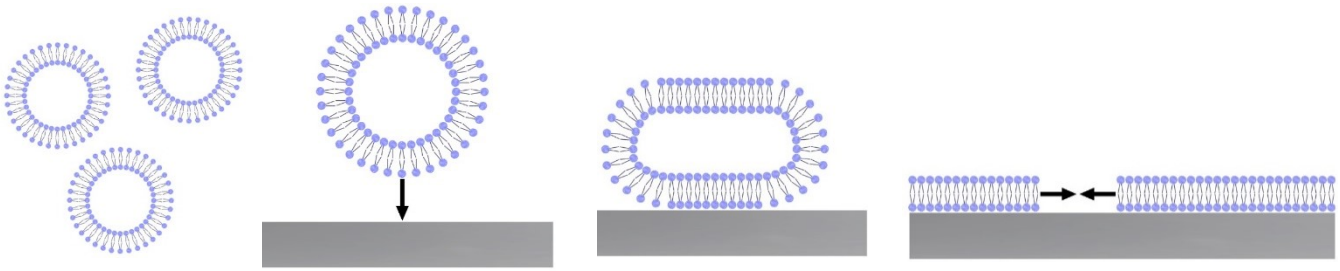

Figure 3.2: Schematic of lipid vesicle deposition, rupture, and fusion to hydrophilic slides.[29]

This process of vesicle fusion is governed by many controllable factors. The pH of the solution along with the charge density and polarity of the lipids can interfere with the lipid vesicles alter the fusion process. Electrostatics dictate the ionic strength, of the lipid solution can also completely block or facilitate vesicle fusion. In this work, vesicles were absorbed onto pretreated glass slides at 150 mM NaCl for 30 minutes.

Purified CD44 transmembrane protein was incorporated into the lipid bilayer using a modified procedure from the Konstantopoulos group.[57] The protein and lipid mixture were dissolved in using Triton X surfactant. Vesicle formation is induced through removal of the surfactant through dialysis.[57] The two main buffer solutions used in this procedure were prepped as follows, 10X Buffer A: 15.76 g Tris HCl, 14.61 g NaCl, 0.555 g $CaCl_2$, 500 mL DI water; Buffer B: 7.2 mL DI water, 800 µl 1x Buffer A, 7.2 µl Triton X100. Lipid Bilayers were prepared by adding 8 mg of POPC lipids (with desired PEG concentration) to Buffer B and extruding 10 times. 330 µl of this lipid solution is added to 130 µl of 80 µg/ml CD44 and incubated for 2 hours under agitation. After incubation, the lipid and protein solution is added to the dialysis cassette and placed in 1L of 1X Buffer A under agitation. The dialysis procedure takes a total of 36 hours, and the buffer solution is changed every 12 hours. At the end of the dialysis period, the lipid solution is removed for the cassette and can be stored for up to 1 month at 4°C. Lipid bilayers with integrated CD44 proteins were deposited onto glass substrates in the same manner as previous bilayers.

Substrate composition also affects monolayer formation. The Corning and Fisher brand glass slides and coverslips used in other experiments contain aluminum ions, creating an unfavorable charge density and water structure. VWR #2 glass cover slips do not contain any aluminum ions and were used in all lipid bilayer experiments. These substrates were cleaned first by sonicating in acetone for 3 minutes, ethanol for 3 minutes, and DI water for 1 minute. The substrates were then transferred into a solution of 1:4 diluted 7X detergent in water, and placed on a 100°C hotplate until the solution reaches the glass transition point and turns clear. Substrates were then rinsed ten times in DI water and heated until the DI water began to boil. Samples were then removed and placed in a piranha solution, a 1:3 mixture of 99% H_2SO_4 and 30% H_2O_2, for exactly 15 minutes. Piranha is a violent oxidizing agent that removes organic contaminants and forms a uniform oxide layer on the glass surface. The substrates were then transferred to fresh DI water, sonicated for two minutes, and rinsed in DI water ten times.

3.2.4 Cell Culture

The MDA-MB-231 Human breast adenocarcinoma cell line was utilized extensively throughout this work. This rapid growth cell line has been thoroughly characterized and has been found to show an overexpression of the transmembrane protein CD44[55,56]. This protein is integral to this work as its involvement in cell-cell interactions has been linked to tumor progression and metastasis [56].

Cell growth medium is prepared by first prewarming 50mL Fetal Bovine Serum (FBS) and 450 mL of Dulbecco's Modified Eagle's Medium (DMEM) to 37°C. These two solutions were sterile filtered using a vacuum into the final

medium flask. The MDA-231 human breast cancer cells were cultured in 75 cm^2 and 150 cm^2 rectangular canted neck flasks using 10 mL and 15 mL of media respectively and maintained in a humidified, 5% CO2 - 95% atmospheric air incubator at 37°C. To maintain cells, media was exchanged every three days by aspirating off old media and re-placed with fresh, pre-warmed media. Cells were passed on a weekly basis. This was accomplished by first removing all media and washing the cells twice with 3mL of PBS. The cells were then coated with 3 mL of 0.25% trypsin-EDTA and allowed to sit in the incubator for 5 minutes or until cells had completely detached from the flask. Once the cells had detached, the trypsin was inactivated by adding the cell-trypsin solution to 6mL of media in a centrifuge tube. Trypsin was further removed by centrifuging the solution at 2500 RPM for 5 minutes at room temperature. After removing the supernatant, the cell pellet was resuspended and gently broken up in 5 mL of media. Using a hemocytometer, cells were counted and adjusted to $5x10^5$ cells/mL.

3.2.5 Immunoprecipitation

Immunoprecipitation is a process of isolating protein antigens from a solution using their specific binding antibody. In this work, we used immunoprecipitation to isolate CD44 proteins from cultured MDA-231 cells. The protocol is one adapted from literature[57].

Cells were prepped for immunoprecipitation by first removing them from flasks and then adding a lysing buffer. To collect mature cells, all reagents were first prewarmed to 37°C. Once cells reach about 80% confluent, 150 cm^2 flasks were washed with PBS. The cells were then gently removed by using 3 mL of enzyme free cell dissociation buffer and incubated for 15 minutes. After incubation, the cells were removed and centrifuged twice, washing with PBS after the first run. All of the supernatant is then removed, and cells were stored at -80°C for up to one month. Before thawing the cell pellets, the cell lysis buffer was prepared by combing 50mL Lysis Buffer A, 2% (v/v) Nonidet P-40, ¼ tablet Protease Inhibitor, and enough PMSF for a final concentration of 20 µg/mL. The Lysis buffer A was prepared by combining 300 mL DI water, 2.63g NaCl, 0.6 mL 0.5 M EDTA, 18 mg Tris-Base, 598.5 µL 10mg/ml PMSF, 3 crushed tablets of Protease Inhibitor, and 0.06g NaN_3, the final dissolved solution was sterile filtered.

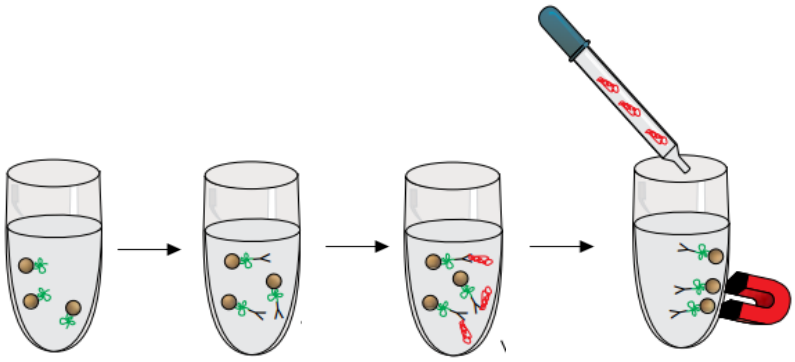

Figure 3.3: Immunoprecipiatation with magnetic Dynabeads. (1) Dynabeads (gold) with Protein G (green) (2) Added antibody (black) sample (3) Added target protein (red) sample (4) Elute to isolate target protein.

When ready for use, the pellets were thawed to room temperature. To start the lysing process, 1 mL of the cell lysis buffer was added to the pellet and the mixture was vortexed for a 10 seconds. The cells and lysis buffer mixture was then

incubated on ice for one hour, vortexing every 15 minutes. Figure 3.3 depicts the immunoprecipitation process. Before adding the lysed cell mixture to the magnetic immunoprecipitation beads, 50 µl of beads were incubated for 10 minutes at room temperature with 200 µl the provided washing and binding buffer and 10 µL of 0.5mg/mL anti-CD44 515 antibody. The supernatant was removed and the beads were resuspended in 500 mL of cell lysate and incubated at room temperature for 2 hours. The tube is then placed on the magnet and the supernatant removed and saved for later use, at this point only the beads, anitbodies, and CD44 proteins remain (bead-Ab-Ag complex). Before the elution steps, the bead-Ab-Ag complex was washed 3 times with 200 µl of the provided washing buffer. CD44 proteins were eluted from the beads through a series of washing steps. Each wash step was done with 300 µl of wash and gentle resuspension by pipetting, and the steps are as follows: 3 times with Wash 1 (buffer A/2% Non Idet-P40/1%BSA), 2 times with Wash 2 (Buffer A/1% Non Idet-P40), 5 times with PBS without Calcium, 1 time with PBS and sodium azide. Following the final wash, the beads-Ab-Ag complex is resuspended in 80 µl of PBS with sodium azide and boiled at 100°C for 10 minutes. The final elutant is collected and stored at 4°C until ready for use.

3.2.6 Protein quantification and Identification

We ensured accurate isolation of the CD44 proteins by detection through Western Blotting. Concentrations of protein in the bilayer was kept consistent by quantifying using a MicroBCA. Because CD44 proteins are around 85 kDa, Western Blots were run on 3%-8% Tris-Acetate gels. Samples were run under reducing conditions and prepared by first combing the loading buffer and reducing

agent at a 5:2 ratio. The reducing agent was added to samples by adding enough to have a final concentration of about 50 µg protein/well. Samples were then denatured by incubating at 70°C for 10 minutes. The gel is set-up by placing into the cartridge and adding 500 mL of running buffer to the chamber. Samples and a standard ladder could then be carefully added to wells, and then run for 1 hour at 150 Volts. At the end of the run, the gel was covered with a cellulose membrane that has been presoaked in the transfer buffer and 1% methanol. The gel and transfer membrane was surrounded by filter paper and placed back into the chamber, which had been filled with 500 mL of transfer buffer. This was run at 150 volts for 2 hours. Once the run is complete, the membrane was removed and washed with a Ponceau Red stain to ensure that the transfer was successful. Before proceeding, the Ponceau Red stain is completely washed off with DI water. The membrane was then left in a 1:100 primary antibody and TBST solution overnight under agitation. Excess antibodies were removed by washing the membrane twice in TBST for 15 minutes under agitation. Proteins were then tagged with a secondary antibody by incubating in a 4:1000 antibody to TBST solution for 1 hour under agitation. Excess secondary antibody was removed through 2 more 15 minute washes in TBST. To prepare for imaging, the membrane was stained with a 1:1 solution of peroxide solution and an enhanced luminol solution and incubated for 3 minutes. Final protein bands are imaged using a Bio-Rad Gel Doc XR+ System.

Micro BCA is a high sensitive colorimetric protein assay technique. Standards of known BSA concentrations (0 µg/µl to 200 µg/µl) are prepared by diluting the 2.0 mg/mL stock. The working reagent was prepared by mixing reagent

MA, reagent MB, and reagent MC in a 25:24:1 ration. Samples are prepped by adding the working reagent to each known and unknown sample at a 1:1 ratio and incubating at 60°C for 1 hour. Using a spectrophotometer, a standard curve is made with the known samples and then unknown concentrations can be determined from this curve.

4. STUDYING INTERACTIONS BETWEEN LIPID BILAYERS, POLYMERS, AND POLYSACCHARIDES

4.1 Introduction

The goal of this chapter is to construct and characterize a model system that uses Diffusing Colloidal Probes to study the HA-CD44 system. The goal is for the model to have a controllable supported lipid bilayer with an integrated polymer brush that facilitates levitation of colloidally stable Hyaluronic Acid modified probes. This was done using previous research (i.e. lipid bilayers, protein-carbohydrate interactions, specific biomolecular binding) to guide the characterization of SLBs with FRAP and Pluronic F108 coated particles as well as the stabilization of HA modified particles.[29,49,50] In order to prove that this model system is an achievable goal, we isolated each of these previous studies before carefully combining them.

The study of intermolecular forces has become increasingly important for understanding the role of proteins, carbohydrates, and other biomolecules in biophysics and medicine. These weak, specific interactions between proteins and carbohydrates influence critical biological functions such as cell-cell adhesion, migration, signaling, proliferation, and metastasis.[1-6] Understanding protein-carbohydrate interactions has become a key challenge in the field of nanomedicine for the development of specific, targeted drug delivery techniques.

Extensive studies have shown a strong relationship between the overexpression of the transmembrane protein CD44 and tumor metastasis.[56,57,78,79] Building off that relationship, much work has been done in order to understand the protein and its main binding target, Hyaluronic Acid.[31,37] Despite, there has been

little done to understand the binding characteristics (i.e. interaction potential, number of bind sites, HA length) of the CD44-HA complex.

The model system in this work is based on a lipid bilayer, for which we utilized 1-palimitoyl-2oleoyl-*sn*-glycero-3-phosphocholine (POPC) lipids, a phosphatidylcholine, to represent the cell membrane (Figure 4.1). While eukaryotic cell membranes are composed of a variety of lipid types, phosphatidylcholines are one of two major, neutral lipids found in the cellular membrane.[72] Phosphatidylcholine molecules, which account for more than 50% of eukaryotic cell membrane lipids, will self-organize spontaneously into a planer bilayer. The cylindrical phosphatidylcholine molecules will self-assemble with the fatty acid tails (with one unsaturated chain) facing each other and polar head groups interfacing with the aqueous phase.[73]

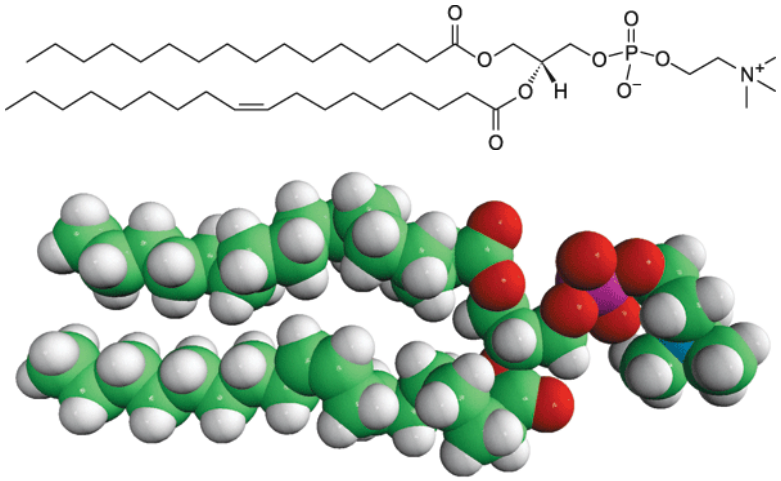

Figure 4.1: Molecular structure and schematic of 1-palimitoyl-2oleoyl-*sn*-glycero-3-phosphocholine.

Phosphatidylcholines have been implicated in collocating membrane proteins and signaling molecules.[74,75] Because of its properties and structure, POPC has been

successfully used in modeling cellular membrane dynamics.[70] Our group has utilized these known cellular dynamics to create a model system for studying kT interactions, a basis for the bulk of this work.[41]

4.2 Theory

In order to characterize our system and quantify our results, video microscopy and TIRM was utilized. Interaction potentials between individual particles and the wall were explained as

$$u_{net}(h) = u_{grav}(h) + u_{VdW}(h) + u_{steric}(h) \quad (4.1)$$

where u_{net} is the sum of the gravitational (u_{grav}), van der waals (u_{vdW}), and steric (u_{steric}) interaction potentials. Because this system is kept at physiological conditions, long range van der Waals interactions are the dominant force and electrostatics can be ignored. The gravitational contribution is a product of the particle weight and its height above the wall, given by

$$u_{grav}(h) = mgh = \frac{4}{3}\pi a^3(\rho_p - \rho_f)gh \quad (4.2)$$

Attractive van der Waals arise from fluctuations in dipoles, and can be explained as

$$u_{vdw}(h) = -aA_{132}(h + h_{wk})^p \quad (4.3)$$

In this system, the Hamaker constant explains the impact of silica-water-silica surfaces and the inverse power law is fit with p = -2.195. The repulsive forces in the form of steric stabilization by polymer brushes are described as

$$u_{steric}(h) = 16\pi a f_M \Delta_0 \Gamma \gamma^{-1} \exp(\frac{-h \cdot \gamma}{2 \cdot \Delta_0}) \quad (4.4)$$

Because we measured interaction potentials between two different types of polymer brushes, the repulsive forces in HA-F108 geometries can be explained with the asymmetric Milner equation given as,

$$u_{asym\ steric}(h) = 8\pi a \Lambda_1^{\frac{\lambda_2}{(\lambda_1+\lambda_2)}} \Lambda_2^{\frac{\lambda_2}{(\lambda_1+\lambda_2)}} (\lambda_1 + \lambda_2) \cdot \exp\left(\frac{-h}{\lambda_1+\lambda_2}\right) \quad (4.5)$$

where $\Lambda_n = \Gamma_n f_{Mn}$ and $\lambda_n = \frac{\delta_n}{\gamma_n}$. All relevant equations utilized in this work are explained in more detail in Chapter 2.

4.2 Materials & Methods

More extensive details of all procedures and materials can be found in Chapter 3. Briefly, this set of experimentation utilized F108 Pluronic, Hyaluronic Acid, and POPC Lipid Bilayers. Silica particles and slides were coated in F108 Pluronic via physiosorbtion and coated with HA via chemiosorption. Lipid bilayers were given additional stability by incorporating PEG into the vesicles before forming uniform layers on slides via vesicle rupture and fusion. In this work we mixed 5 mg of POPC lipids dissolved in chloroform with enough PEG2000 and DiA for a final concentration of 91% POPC, 8% PEG2000, and 1% DiA. After drying, this mixture was reconstituted in DI water, subjected to 10 freeze/thaw cycles in liquid nitrogen, and finally extruded 10 times. Bilayers were allowed to form for 30 minutes on Pirahna cleaned slides by adding 60 µl of lipids and 60 µl of 150 mM NaCl to an O-ring. Before adding particles for experiments, excess lipid

vesicles were removed with PBS washes. Fluorescent lipid bilayers were imaged quantitatively on a confocal microscope using a 488 nm argon laser.

4.4 Results & Discussion

4.4.1 Steric Levitation of F108 Pluronic and Hyaluronic Acid Coated Particles

Under physiological conditions (150 mM NaCl), van der Waals attraction will cause bare silica particles to stick to surfaces. To mitigate this, we have shown the coating both particles and walls with Pluronic F108 we can create stable, diffusing colloidal probes that allow us to study kT scale interactions. Because we will be incorporating PEG into the lipid bilayers, we can use this Pluronic F108 model as a positive control for comparison[71]. Figure 4.1a shows the geometry of the coated particle-wall ensemble used in the TIRM measurements of this work. We were able to sterically stabilize 2.3 μm Pluronic F108 coated silica particles in physiological conditions over a silica substrate also coated in Pluronic F108.

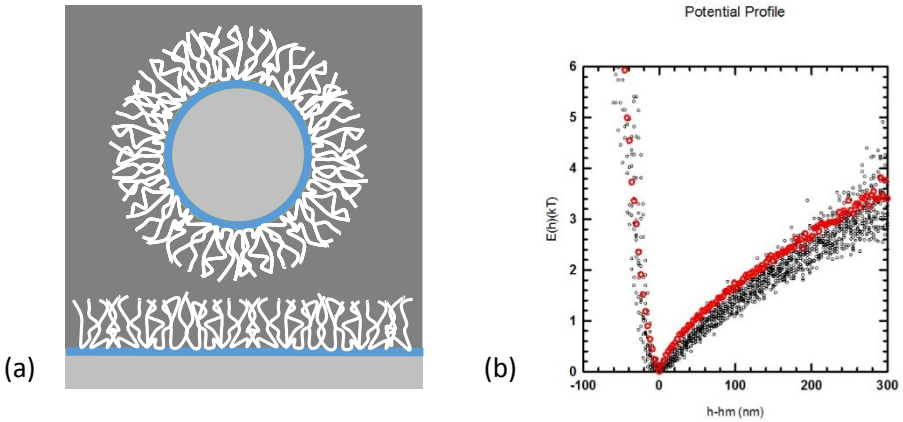

Figure 4.2: (a) Schematic of the geometry of both the glass substrate and the silica particle modified with octadecanol (blue) and physisorbed F108 (white) and its associated interaction potential profile (b) derived from TIRM data. Black dots are individual particle profiles and the red dots represent the ensemble average.

While fairly simple, it was important that we continue to ensure that the most basic of measurements is reproducible with a high level of confidence. By fitting our data to the theoretical curve, our values (Table 4.1 and Figure 4.3) agree with those of previous findings.

Table 4.1: Parameters to fit the interaction potential of Pluronic F108 particles on a Pluronic F108 coated wall to a theoretical curve.

Δ_0	f_0	H_{wk}
18 nm	70	8 nm

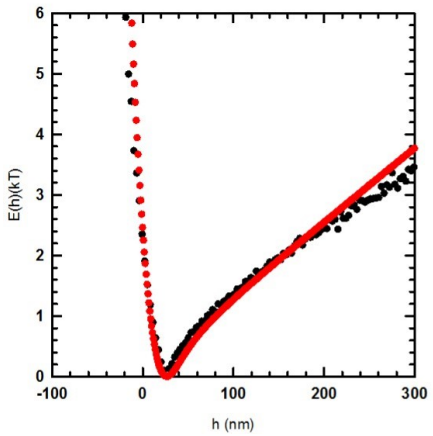

Figure 4.3: Ensemble average interaction profile (black) of Pluronic F108 particles on a Pluronic F108 wall potential profile date fit to a theoretical curve (red).

By following a previously detailed protocol, but eliminating the use of PEG as an additional stabilizer resulted in poor particle stability (Figure 4.4b). While the added PEG layer increases colloidal stability (Figure 4.4a), it decreases the amount of HA and interferes with purely HA-CD44 interactions.

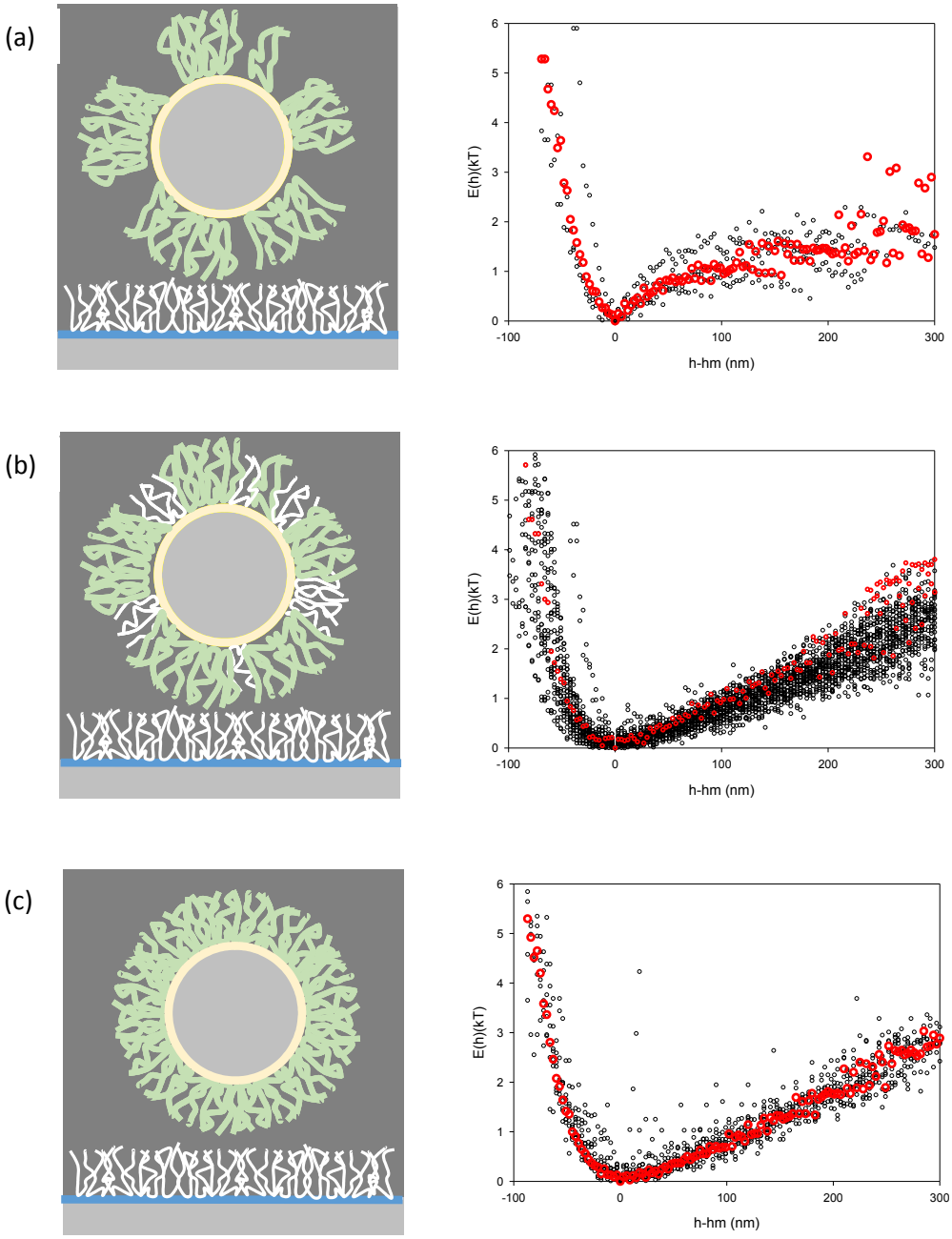

Figure 4.4: Comparison of the stability of various methods of grafting HA (green) onto APTES (yellow) modified particles. (a) Schematic of HA coated particles using the previous method, over F108 (white) and its associated potential energy profile. (b) schematic of HA coated particles enhanced with F108 in accordance with a previous procedure, and its associated potential energy profile (c) schematic of HA coated particle with new procedure and its associated potential energy profile. In each potential profile, the black dots are individual particle profiles while the red in the ensemble average.

In order to remove the additional PEG coating, we focused on the HA grafting conditions. Due to the large size of HA (~100kDa), we found that by first allotting time for the HA conjugate to the surface and then collapsing the long HA chains with a high molar salt (2M NaCl) we were able to graft a denser layer of HA. This denser layer of HA provides enough steric stabilization to eliminate the need for any additional polymer stabilization with PEG, as in demonstrated in Figure 4.4c. In order to confirm our new procedure and test its robustness, we were able to show that previously stable F108 particles were levitated over an HA modified wall, and HA modified particles were stably levitated over an HA modified wall. The confirmation of these results can be seen in Figure 4.5 and Figure 4.6, and the fitting values were compared in Table 4.2. Validating the stability of HA coated particles over an F108 brush also provides a point of comparison in the next stage where PEG is incorporated into lipid bilayers.

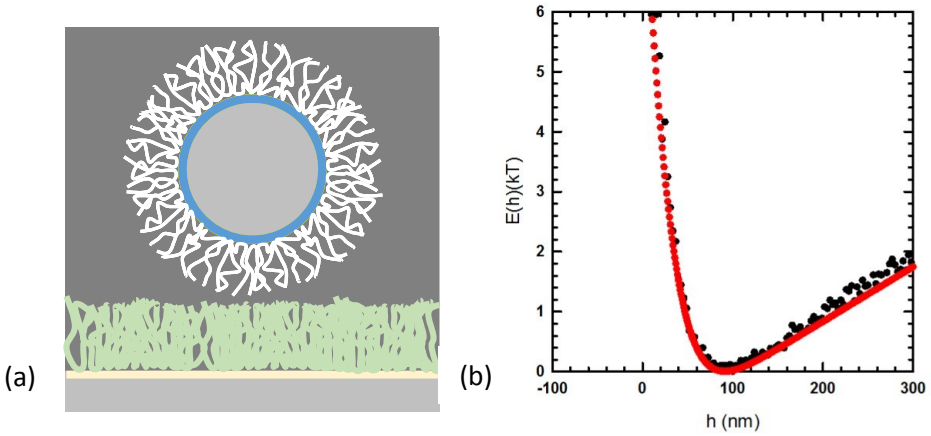

Figure 4.5: (a) Schematic of the geometry of octadecanol (blue) modified silica particles coated with Pluronic F108 (white) coated particles over a surface modificed with APTES (yellow) and HA (green) and its (b) associated interaction potential energy profile fit to a theoretical curve where the red dots represent the theoretical fit and the black dots are the ensemble average.

(a) 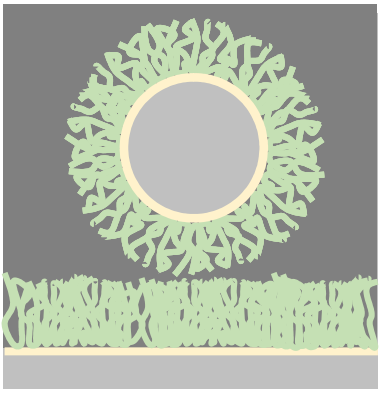 (b) 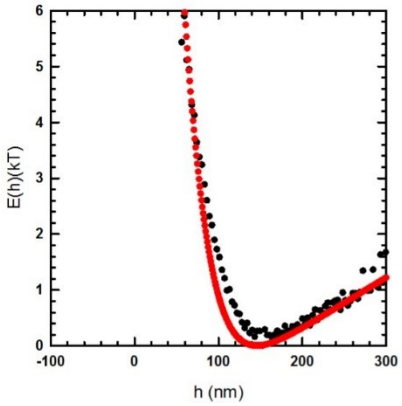

Figure 4.6: (a) **S**chematic of HA coated particles over an HA coated wall and its (b) associated potential profile fit to a theoretical curve where the red dots represent the theoretical fit and the black dots are the ensemble average.

Table 4.2: Comparison of parameters used to fit TIRM data of average potential energy profiles to a theoretical curve. Parameters are fit to equation 4.1 for symmetric geometries (F108-F108, HA-HA) and equation 4.5 for asymmetric geometries (F108-HA).

Geometry	δ_1 (nm)	δ_2 (nm)	f_1	f_2	h_{wk} (nm)
F108-HA	120	14	15	70	20
HA-F108	155	18	30	70	20
HA-HA	180	-	30	-	5

4.4.2 Lipid Bilayer formation

Supported lipid bilayers with an incorporated polymer brush have been utilized to study surface immobilized proteins and biomolecules[39]. In this work, we aim to utilize the same lipid bilayer system to study transmembrane proteins. Before incorporating proteins into the bilayer, we sought to prove the stability and optimize the bilayer system. A previously developed procedure was further optimized under our lab conditions by investigating both the concentration of PEG in the bilayer and the concentration of salt used to facilitate vesicle rupture and fusion to silica

substrates. Previous work had utilized very high salt solutions (~0.7M $MgSO_4$) to facilitate bilayer formation.

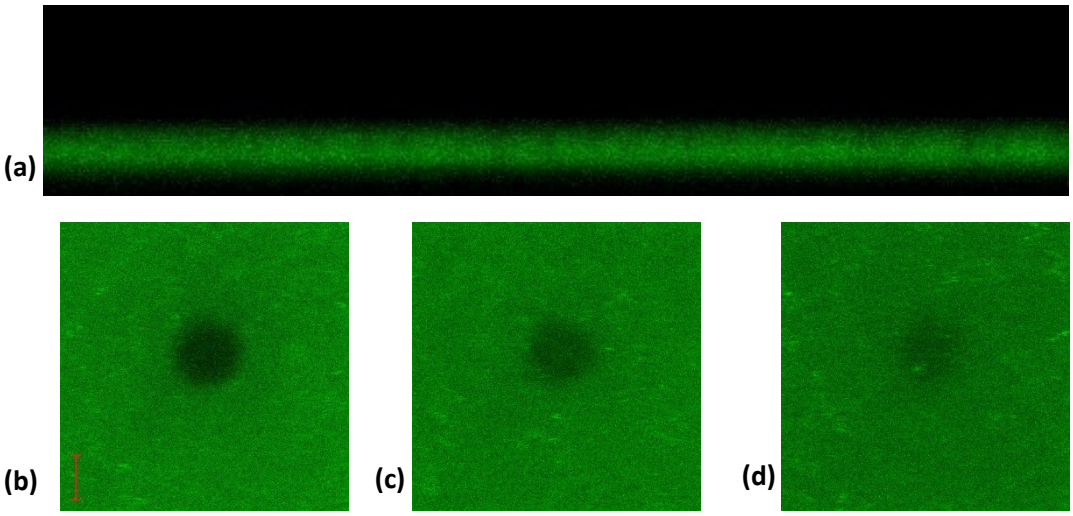

Figure 4.7: Qualitative confirmation of the fluorescent lipid bilayer using confocal microscopy. (a) Cross section of fluorescent lipid bilayer. (b), (c), & (d) t=0min, 3min and 7 min of FRAP experiment. Scale bar: 2μmd

Throughout this work, we found that such a high concentration of salt was dehydrating the surface and preventing lipid vesicles from fusing to the underlying substrate. Instead we found that lower salt strengths, and physiological strength in particular, were sufficient in facilitating vesicle fusion. Formation of a complete lipid bilayer was qualitatively confirmed using FRAP and levitation of stable F108 particles (Figure 4.7). Table 4.3 details the influence of salt strength of lipid bilayer formation. The thickness of the expected 5nm lipid bilayer cannot be accurately measured due to diffraction limitation. The wavelength of emitted light (488nm) is much larger than that of the bilayer, so accurate resolution cannot be achieved. Diffraction limitation is why confocal imaging was used only as a qualitative tool.

Table 4.3: Influence of various salt strengths on lipid bilayer formation.

Ionic Strength Range	pH range	Bilayer Formation
0-50 mM NaCl	7-8	No fusion
0-50 mM $MgSO_4$		
0-50 mM NaCl	11-12	No fusion
0-50 mM & $MgSO_4$		
100-300 mM NaCl	**7-8**	**Fusion**
100-300 mM $MgSO_4$		
700-1000 mM NaCl	7-8	No Fusion
700-1000 mM $MgSO_4$		
700-1000 mM NaCl	11-12	No Fusion
$MgSO_4$		

With a confirmed method of lipid bilayer formation, we were also able to optimize the amount of incorporated PEG. Different concentrations were tested by determining the percentage of levitated stable F108 coated particles. Results are detailed in Table 4.4.

Table 4.4: Varying concentrations of PEG in the lipid bilayer and their effect on colloidal stability.

PEG Concetration	Colloidal Stability
0%	No particle levitation
2%-5%	No particle levitation
7%	**75% particles levitation**
8%	**>90% particle levitation**
9%	**75% particle levitation**
10%-20%	Minimal particle levitation

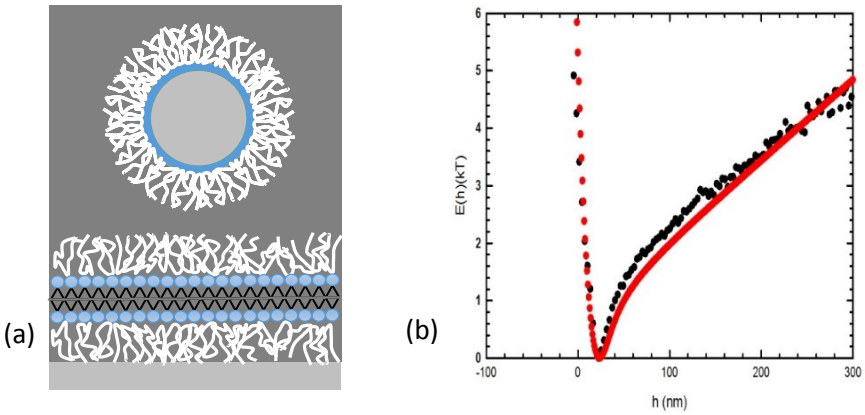

Figure 4.8: (a) Schematic of an PEG coated particle over a lipid bilayer with 8% integrated PEG (white) and its (b) associated potential energy profile fit to a theoretical curve where the red dots represent the theoretical fit and the black dots are the ensemble average.

The optimization of these two parameters now provided us with a well understood platform to start to create our model cell system. As seen in Figure .8, steric stability of our optimized bilayer was confirmed by levitating PEG modified particles.

To build out our model system, we needed to ensure the stability of our polysaccharide of high interest (HA) over the lipid bilayer. Figure 4.9 and Table 4.5, shows that the optimization of both the lipid bilayer formation and the HA grafting has given us a high stable colloidal system.

Table 4.5 Comparison of parameters used to fit TIRM data of average potential energy profiles to a theoretical curve. Parameters are fit to equation 4.1 for symmetric geometries (F108-POPCand equation 4.5 for asymmetric geometries (HA-POPC).

Geometry	δ_1 (nm)	δ_2 (nm)	f_1	f_2	h_{wk} (nm)
F108-POPC	-	18	-	70	8
HA-POPC	155	18	15	70	20

(a)

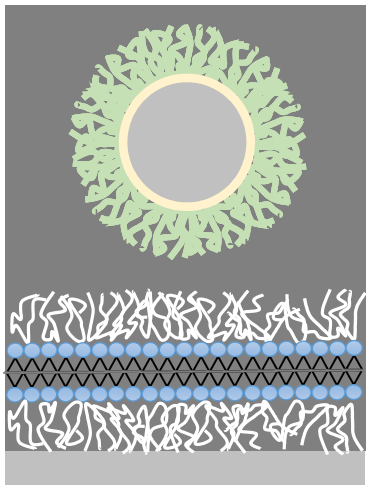

(b)

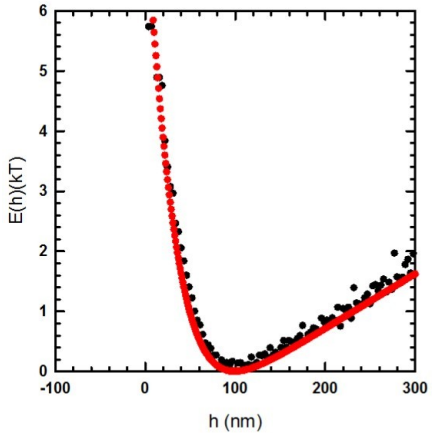

Figure 4.9: (a) Schematic of an HA coated particle over a lipid bilayer with 8% integrated PEG (white) and its (b) associated potential energy profile fit to a theoretical curve where the red dots represent the theoretical fit and the black dots are the ensemble average.

4.5 Conclusions

We were first able to confirm previously shown work with stabilizing PEG and HA modified particles as well as a lipid bilayer system. By eliminating the secondary PEG stabilization of HA modified particles, we are able to now completely isolate the HA to study its interaction with CD44 proteins. The optimization of the lipid bilayer system gives us insight as to how much we can alter the PEG concentration to accommodate different concentration of CD44 proteins while still maintaining a fluid, stable bilayer. Finally, by measuring the interaction of HA modified particles over a lipid bilayer, we can use that as a point of comparison to study a model cell system of the interactions of HA and CD44 that has been incorporated into a lipid bilayer.

5. STUDYING INTERACTIONS BETWEEN HYALURONIC ACID AND CD44 TRANSMEMBRANE PROTEINS IN A MODEL CELL SYSTEM

5.1 Introduction

The intermolecular forces between proteins, carbohydrates, and other biomolecules have become increasing important in understanding their role in biophysics and medicine. These weak, specific interactions between proteins and carbohydrates influence critical biological functions such as cell-cell adhesion, migration, signaling, proliferation, and metastasis.[1-6] Understanding protein-carbohydrate interactions has become a key challenge in the field of nanomedicine for the development of specific, targeted drug delivery techniques.

Extensive studies have been done on the structure and function of a vast array of proteins and carbohydrates. Specifically, the transmembrane protein CD44 and its main binding target, Hyaluronic Acid (HA), have become a very relevant interaction complex in cancer research.[59,60] CD44, a widely expressed cell-surface glycoprotein, exists in many isoforms and is an important factor in cell adhesion, proliferation, migration, and other essential cell functions.[59,61] With its integral role in regulating many cellular functions, CD44 has been implicated in a number of diseases, especially cancer.[56,59-62] CD44's principal ligand, HA, has also been implicated for its inflammatory and tumorigenic responses.[61.65] HA is a ubiquitous glycosaminoglycan of the extra cellular matrix, and binds to the signal transducing CD44 receptors to play a major role in cell adhesion, motility, and proliferation.[64]

In this work, we isolated CD44 proteins from MDA-MB-231 Human breast cancer cells. The MDA-MB-231 cell line has been studied extensively as a metastatic model system.[76] More relevant to this work, the MDA-MB-231 cell line has been found to express CD44 at levels that are over 30% higher than normal cells.[77] These cells predominantly express $CD44^{+}$, the form of the protein that has been shown to have the closes link to tumor progression and invasion.[77] With these properties, we look to incorporate these ideal transmembrane proteins into our lipid bilayer system to develop a controlled cellular model system.

Lipid bilayer systems have been well studied as model systems, and have been utilized to study CD44-HA binding kinetics.[57] Despite this, there lacks a model system to study the multivalent interactions of the CD44-HA complex. In this chapter, we look to verify previous measurements of CD44-HA interactions on live cells by creating a model cell system to measure the multivalent interactions of the CD44-HA complex.[50] This was done by first isolating and integrating CD44 into the lipid bilayer and confirming its stability by comparing it to measurements detailed in Chapter 4. We then studied various conditions to induce or block CD44-HA binding.

5.2 Theory

In order to characterize our system and quantify our results, video microscopy and TIRM was utilized. Interaction potentials between individual particles and the wall were explained as

$$u_{net}(h) = u_{grav}(h) + u_{VdW}(h) + u_{steric}(h) \qquad (5.1)$$

where u_{net} is the sum of the gravitational (u_{grav}), van der waals (u_{vdW}), and steric (u_{steric}) interaction potentials. The gravitational contribution is a product of the particle weight and its height above the wall, given by

$$u_{grav}(h) = mgh = \frac{4}{3}\pi a^3(\rho_p - \rho_f)gh \tag{5.2}$$

Attractive van der Waals arise from fluctuations in dipoles, and can be explained as

$$u_{vdw}(h) = -aA_{132}(h + h_{wk})^p \tag{5.3}$$

The repulsive forces in the form of steric stabilization by polymer brushes are described as

$$u_{steric}(h) = 16\pi a f_M \Delta_0 \Gamma \gamma^{-1} \exp(\frac{-h \cdot \gamma}{2 \cdot \Delta_0}) \tag{5.4}$$

Because we measured interaction potentials between two different types of polymer brushes, the repulsive forces in HA-F108 geometries can be explained with the asymmetric Milner equation given as,

$$u_{asym\ steric}(h) = 8\pi a \Lambda_1^{\frac{\lambda_2}{(\lambda_1+\lambda_2)}} \Lambda_2^{\frac{\lambda_2}{(\lambda_1+\lambda_2)}} (\lambda_1 + \lambda_2) \cdot \exp\left(\frac{-h}{\lambda_1+\lambda_2}\right) \tag{5.5}$$

where $\Lambda_n = \Gamma_n f_{Mn}$ and $\lambda_n = \frac{\delta_n}{\gamma_n}$. All relevant equations utilized in this work are explained in more detail in Chapter 2.

5.3 Materials & Methods

More extensive details of all procedures and materials can be found in Chapter 3. Briefly, this set of experimentation utilized F108 Pluronic, Hyaluronic Acid, and POPC Lipid Bilayers, cell culture, immunoprecipitation, and protein

quantification and identification. Silica particles and slides were coated in F108 Pluronic via physiosorbtion and coated with HA via chemiosorption. Lipid bilayers were given additional stability by incorporating PEG as well as CD44 proteins into the vesicles before forming uniform layers on slides via vesicle rupture and fusion. In this work we mixed 8 mg of POPC lipids dissolved in chloroform with enough PEG2000 and DiA for a final concentration of 91% POPC, 8% PEG2000, and 1% DiA. After drying, this mixture was reconstituted in the Buffer B solution, subjected to 10 freeze/thaw cycles in liquid nitrogen, and finally extruded 10 times. CD44 proteins were integrated into the lipid vesicles through dialysis. 130 µl of 80µl/ml CD44 protein was added to 440 µl of 8 mg/ml lipids in Buffer B. This mixture was then put into a dialysis cassette and put in the Buffer A solution for 36 hours. The buffer solution was changed every 12 hours. Bilayers with CD44 were allowed to form for 30 minutes on Pirahna cleaned slides by adding 60 µl of lipids and 60 µl of 150 mM NaCl to an O-ring. Before adding particles for experiments, excess lipid vesicles were removed with PBS washes. CD44 proteins were isolated via immunoprecipitation with magnetic beads from cultured MDA-231 cells. The proteins were then identified with a Western Blot and quantified with MicroBCA.

5.4 Results & Discussion

With the well characterized and stable lipid bilayer model system from Chapter 4, we then looked to create a model system of CD44-HA interactions.

5.4.1 Isolation, Identification, and Quantification of CD44 proteins

After culturing MDA-MB-231 cells, which have elevated levels of CD44 expression, we were able to successfully extract isolated CD44 proteins through immunoprecipitation. Each immunoprecipitation was quantified using MicroBCA analysis, where we were able to extract an average of 80 µg/ml of protein. We then ensured that we extracted CD44 proteins by performing a Western Blot under reducing conditions. As seen in Figure 5.1, in a series binding times and elution conditions, we were able to isolate ~85 kDa C D44 proteins.

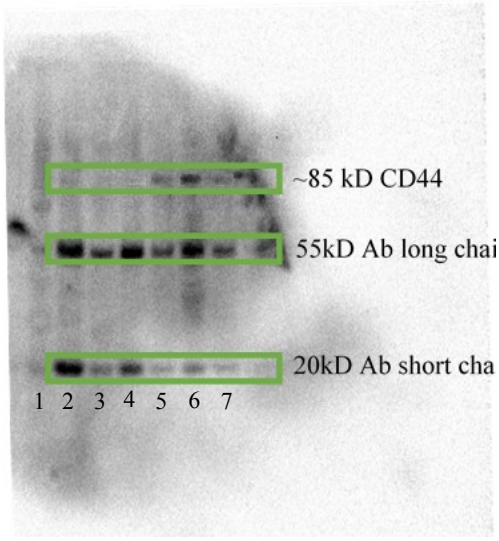

Figure 5.1: Western Blot analysis of CD44 proteins. Lane 1 is a standard ladder, from left to right, the successive lanes are experiments done in groups of two. In the first set (lanes 2&3), the cell lysate was incubated with the beads for 24 hours, the second (lanes 4&5) set for 1 hour and the third set (lanes 6&7) for 2 hours. Within each set of two, the first lane was eluted with a denaturing method and the second with a simpler non denaturing method. The green boxes highlight the CD44 protein and the long and short chains of the antibody.

5.4.2 CD44 Incorporation into Lipid Bilayers

Because CD44 is a transmembrane protein, prepared lipid vesicles were mixed with isolated proteins and dialyzed with a light surfactant. Triton X-100 is a non-ionic surfactant that will not denature the proteins; by dialyzing the lipids with this surfactant, we can expect to incorporate our membrane proteins in their natural conformation.[80] To ensure that uniform, stable bilayers would still form under different buffer conditions, we tested the stability of our system with both Pluronic F108 and HA coated particles. Figure 5.2 depicts both potential energy profiles and their respective fitting parameters are compared in Table 5.1. Through visual inspection, the HA coated particles did not appear to be laterally diffusing, but as seen in Figure 5.2 the associated potential energy profile shows that they are stably levitated.

Table 5.1: Comparison of parameters used to fit TIRM data of average potential energy profiles to a theoretical curve. Parameters are fit to equation 5.1 for symmetric geometries (F108-POPCand equation 5.5 for asymmetric geometries (HA-POPC).

Geo-Buffer	δ_1 (nm)	δ_2 (nm)	f_1	f_2	h_{wk} (nm)
F108-PBS	-	18	-	70	8
HA-PBS	155	18	15	70	20
F108-Buffer	-	18	-	70	10
HA-Buffer	120	14	20	70	20

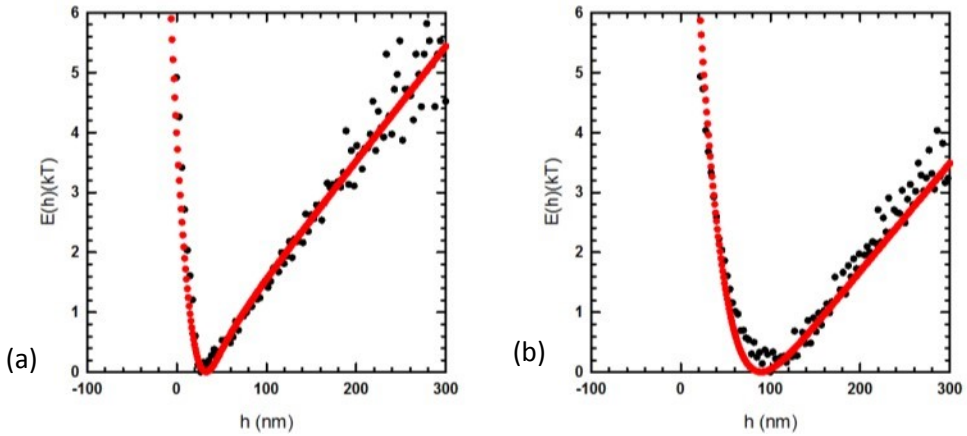

Figure 5.2: Potential energy profiles derived from TI RM data of (a) Pluronic F108 particles and (b) HA particles, both over lipid bilayers that were reconstituted in a surfactant containing buffer and have been dialyzed. Red dots represent the theoretical fit and the black dots are the ensemble average.

To then ensure that in a different buffer solution, our bilayer formed an even monolayer and maintained similar fluidity, we did qualitative analysis with confocal imaging (Figure 5.3).

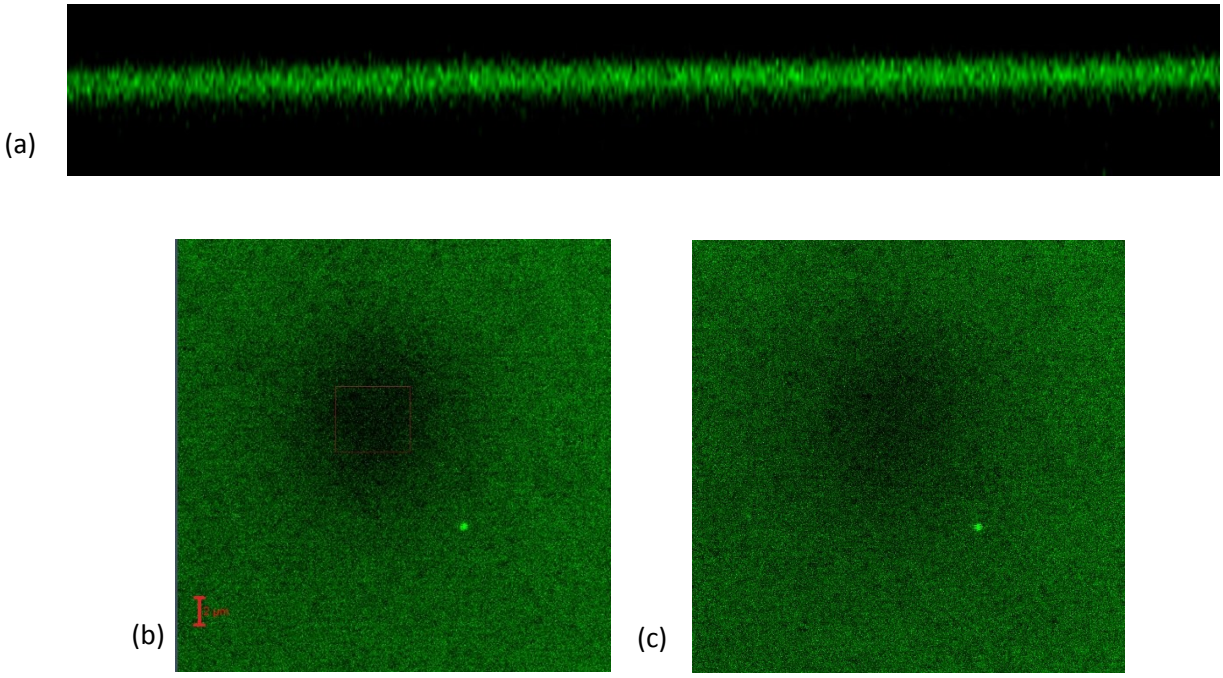

Figure 5.3: Qualitative confirmation of the fluorescent lipid bilayer using confocal microscopy. (a) Cross section of fluorescent lipid bilayer. (b) & (c) t=0min and t=2min of FRAP experiment. Scale bar: 2 µm.

The colloidal stability of the CD44 bilayer was tested by ensuring that Pluronic F108 coated particles levitated over the bilayer and then comparing the potential profiles to those from Chapter 4 under the same conditions. The particle wall geometry and its associated potential profile is depicted in Figure 5.4 and Table 5.2 compares the fitting parameters of Pluronic F108 particles over lipid bilayers with and without CD44 proteins.

Table 5.2: Comparison of parameters used to fit TIRM data of average potential energy profiles to a theoretical curve. Parameters are fit to equation 5.1 for symmetric geometries.

Geometry	Δ_0	f_0	h_{wk}
F108-POPC	18	70	8
F108-POPC+CD44	16	70	10

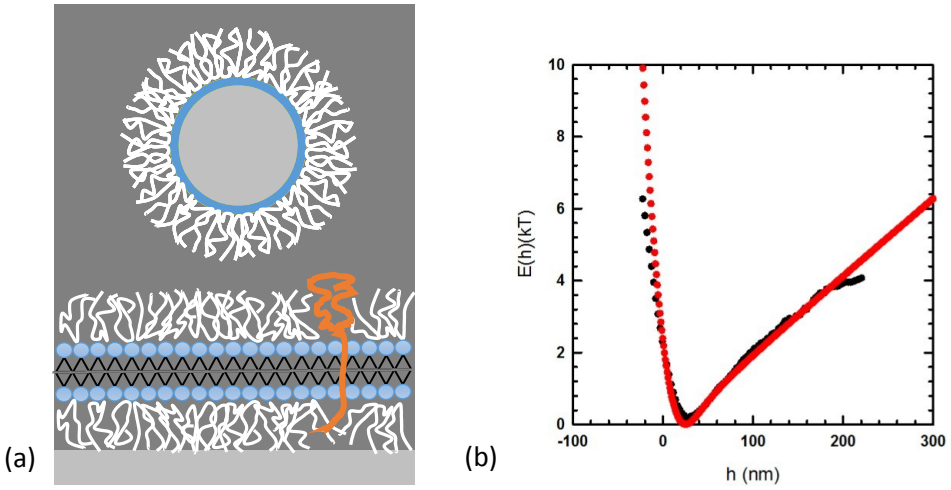

Figure 5.4: (a) Schematic of F108 particles over an 8% PEG lipid bilayer with incorporated transmembrane proteins (orange) and (b) its associated potential profile fit to theoretical curve, where the red dots represent the theoretical fit and the black represent the ensemble average.

5.4.3 Hyaluronic Acid Interactions with CD44

With well characterized lipid bilayer that has been proven stabile following the incorporation of the transmembrane protein CD44, we looked to study the specific HA-CD44 interaction. From previous work and studies, HA is expected to bind to the CD44 transmembrane proteins.[60] We found that HA coated particles were not levitated over the lipid bilayers with CD44 proteins. HA particles also appeared to congregate in certain areas. This could indicate that not only are the HA particles binding to the CD44 proteins, but the CD44 proteins cluster to form lipid rafts. The geometry of this system and the clusters of HA particles over the lipid bilayer with their associated potential energy profile is depicted in Figure 5.5.

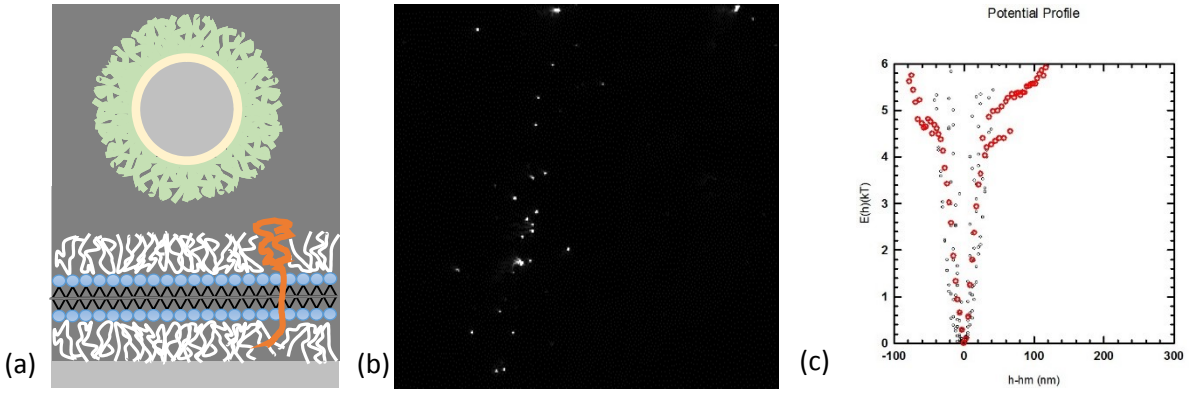

Figure 5.5: (a) Schematic of HA coated particles over a 8% PEG lipid bilayer with CD44, (b) TIRM image of clustered HA coated particles (white) over a lipid bilayer with CD44, and (c) associated potential energy profile of stuck particles where the black dots represent individual particle profiles and the red is the ensemble average.

To further characterize this system, we looked to determine conditions which would induce HA binding reversibility. To do this, we looked at different conditions of bulk solution to create competition amongst the HA binding domains. Because the binding of HA to CD44 is multivalent, adding additional free HA to the bulk solution will create competition in the probability of binding events. In this work, we added 1 mg/ml, 2 mg/ml, and 5 mg/ml of 100 kDa HA to the bulk solution. Figure 5.6 depicts the potential energy profiles of each of these conditions, and indicate that higher concentrations of free HA in the bulk create conditions for HA coated particles to be stably levitated.

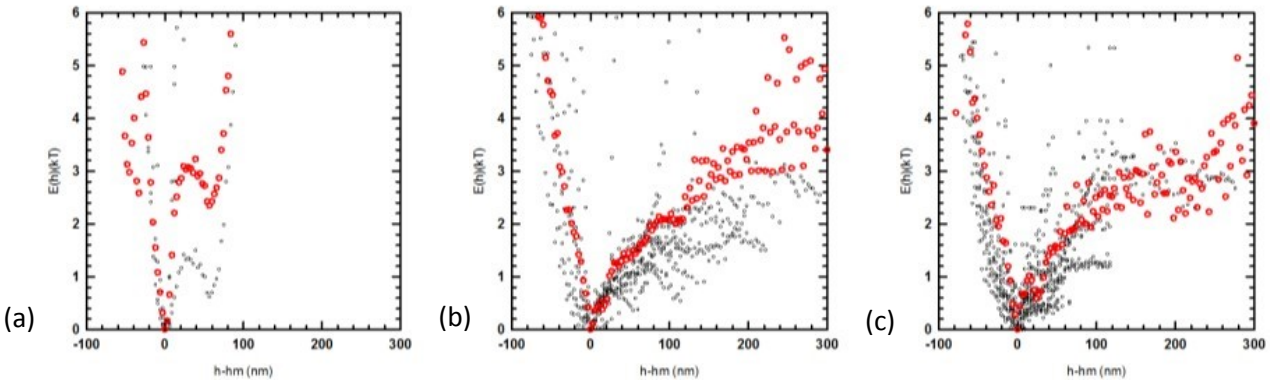

Figure 5.6: 100 kDa HA coated particles over a lipid bilayer containing CD44 proteins, the bulk free HA concentrations are (a) 1mg/ml, (b) 2mg/ml, and (c) 5mg/ml. The black dots represent individual particles and the red is the ensemble average.

5.5 Conclusion

With data from the previously characterized bilayer, we were able to demonstrate that a similarly stable lipid bilayer can be established in a buffer solution containing surfactants. After successfully insolating the CD44 transmembrane protein, it was incorporated into the lipid bilayer. This bilayer was also demonstrated to form evenly and stably. After successfully showing that this

bilayer was stable, we studied the interactions of HA and CD44. We found that 100 kDa HA coated particles congregate to specific areas, indicating that they are binding to the CD44 proteins. The larger areas of concentrated particles also indicate that the CD44 proteins could be congregating together to form lipid rafts. To provide a platform for further research, we looked to exploit the multivalent nature of the HA molecules. By adding varying concentrations of free 100 kDa HA to the bulk solution, it was demonstrated that higher concentrations of HA (>2mg/ml) creates enough competition that HA coated particles do not selectively bind to the CD44 proteins.

6 CONCLUSIONS

Understanding the weak, specific interactions between proteins and carbohydrates has been the main challenge in furthering the development of targeted drug delivery techniques. The interaction between the transmembrane protein CD44 and the common polysaccharide Hyaluronic Acid, has become increasing significant in the study of cancer metastasis. In order to study the multivalent nature of CD44-HA interactions on the kT scale, the work presented aims to develop and characterize a lipid based model cell system.

Before developing the supported lipid bilayer system we optimized the particular modification techniques in a well characterized Pluronic F108 system. Previous work has utilized HA modified particles that were colloidaly stable only with an additional layer of Pluronic F108. By altering the ionic strengths of particle modification steps, we were able to demonstrate through the potential energy profiles produced by TIRM data that HA modified particles can be colloidaly stable and reproducible.

Supported lipid bilayers comprised of POPC lipids were chosen as a model cell system because they are a major component of cellular membranes. By incorporating PEG into the upper and lower portions of the supported lipid bilayers, we were able to establish a high level of stability. This prevented any non-specific interactions between the colloids and the underlying wall. It was found that both pH and Ionic strength of solutions play in significant role in mediating bilayer formation. Neutral pHs (7-8) and mid-range ionic strengths (100mM-300mM NaCl) result in the most uniform bilayers. The uniformity and fluidity of the

supported lipid bilayers was qualitatively confirmed with FRAP. Having established a uniform supporter lipid bilayer, we were then able to confirm its stability. With incorporated PEG concentrations of 7%-9%, potential energy profiles of Pluronic F108 and HA particles over the bilayer demonstrate that the system is reproducible and stable.

Isolation of the CD44 protein was done successfully through immunoprecipitation. Cultured MDA-231 cells, which have been shown to express high levels of CD44 proteins, were used to immunoprecipitate CD44 proteins, and was confirmed by Western Blotting. Because CD44 is a transmembrane protein, we incorporated these isolated proteins into the lipid vesicles by dialysis with a gentle surfactant. The introduction of a surfactant into the system did not affect the stability of the system, as was confirmed through TIRM data of Pluronic F108 particles over dialyzed lipids without CD44. Incorporating CD44 proteins into the supported lipid bilayer also did not affect the stability of the system, this was demonstrated by comparing the potential energy profiles on Pluronic F108 particles over lipid bilayers with and without CD44 proteins.

The specific binding of HA modified particles to CD44 was observed through TIRM. 100 kDa HA coated particles appear to formed clusters of stuck particles over regions of CD44 proteins, as was expected. This could indicate that not only is HA binding to CD44, but the CD44 proteins are also clustered together in lipid rafts. The robustness of this system was further demonstrated by inducing conditions that would inhibit HA-CD44 binding. The addition of 2mg/ml and 5mg/ml free 100 kDa HA to the bulk solution created competition of the HA

binding domains. The TIRM data under these conditions resulted in potential energy profiles that show HA modified particles were stable above the lipid bilayer.

Based on the findings in this work, a supported lipid bilayer based model cell system can be used to study the *kT* scale interactions of CD44 and HA. The measurements and observations presented here demonstrate that a PEG reinforced lipid bilayer system is highly stable and easily modified with various concentrations of PEG and CD44. Specific interactions between CD44 and HA have been shown to exhibit the expected binding characteristics and their binding is reversible. By demonstrating that the binding of HA to CD44 can be inhibited, we have set up a robust platform for further characterization of the CD44-HA binding complex.

7 Future Work

7.1 Further Exploitation of the Robustness of the System

The promising results in Chapter 5 suggest that there are a multitude of techniques to inhibit the binding of CD44 to HA. Research into these parameters would further demonstrate the robustness and limits of this system. All HA used in this work was 100kDa, a large enough polymer that can cause the bulk to become viscous if highly concentrated. Current work is underway to demonstrate HA binding inhibition under various conditions of free HA concentrations and sizes. We are also looking into other inhibitors, such as antibodies, to induce the same results and determine the limits of our system. These results can then be compared to *in vivo* cell measurements to demonstrate that we have developed a very robust model cell system that is replicable, tunable, and comparable to *in vivo* cells.

7.2 Characterization of the CD44-HA binding properties

For the control system demonstrated in this study, all sources of HA were 100kDa in size and all CD44 were of the CD44s isoform. Having demonstrated that this system is robust, the physical binding properties of the CD44-HA binding complex can be explored. CD44 exists in at least 10 isoforms, each having various expression levels in cancerous cells. These isoforms are currently being cultured from cancerous cell lines with high levels of CD44v expression. Physical parameters of the CD44-HA binding complex can be furthers studied to determine selectivity amongst CD44 variants and various sizes of HA. These results can be further confirmed by measuring *in vivo* particle-cell interactions. Thorough

characterization of the binding properties of various isoforms of CD44 and sizes of HA will provide a wide library of knowledge as we look to induce highly selective binding in drug delivery.

7.3 Demonstration of HA particles as a Target Drug Delivery Technique

Following the aforementioned studies, we can then look to use HA modified probes as a target drug delivery technique. With the known binding properties of CD44-HA, we can physically control and induce selectivity. Further exploitation of HA's multivalent nature can allow us to modulate the binding strength of HA to specific isoforms of CD44. By studying this tunable system *in vivo,* we can look to target specific cancer types based on its predominantly expressed form of CD44.

8 REFERENCES

1. Toole, B.P. Hyaluronan: from extracellular glue to pericellular cue. *Nat Rev Cancer*, **2004**. *4*(7): 528-39.

2. Spicer, A.P., Tien, J.Y. Hyaluronan & morphogenesis. *Birth Defects Res C Embryo Today*, **2004**. *72*(1): 89-108.

3. Yang, B.H., C.L. Hall, B.L. Yang, R.C. Savani, and E.A. Turley. Identification of a Novel Heparin-Binding Domain in Rhamm and Evidence That It Modifies Ha Mediated Locomotion of Ras-Transformed Cells. *Journal of Cellular Biochemistry*, **1994**. *56*(4): 455-468.

4. Assmann, V., D. Jenkinson, J.F. Marshall, and I.R. Hart. The intracellular hyaluronan receptor RHAMM/IHABP interacts with microtubules and actin filaments. *Journal of Cell Science*, **1999**. *112*(22): 3943-3954.

5. Lindhorst, T.K. Essentials of carbohydrate chemistry and biochemistry. 3rd ed **2007**: Wiley.

6. Collins, B.E. and J.C. Paulson, Cell surface biology mediated by low affinity multivalent proteinglycan interactions. *Curr. Opinion Chem. Biol.*, **2004**. *8*: 617-625.

7. Hilt, J. Z.; Byrne, M. E. Configurational biomimesis in drug delivery: Molecular imprinting of biologically significant molecules. *Advanced Drug Delivery Reviews*. **2004.** *6*: 1599-1620.

8. Bareford, L. M.; Swaan, P. W. Endocytic mechanisms for targeted drug delivery. *Advanced Drug Delivery Reviews*. **2007.** *59*: 748-758.

9. Homola, J. Present and future of surface plasmon resonance biosensors. *Analytical and Bioanalytical chemistry* **2003.** *377:* 528-539.

10. Cho, K.; Wang, X.; Nie, S.; Chen, Z. G.; Shin, D. M. Therapeutic nanoparticles for drug delivery in cancer. *Clinical cancer research : an official journal of the American Association for Cancer Research* **2008.** *14*: 1310-1316.

11. Evans, E. Probing the Realtion Between Force-Lifetime-and Chemistry in Single Molecular Bonds. *Annu. Rev. Biophys*. *Struct*. **2001**. *30*: 105-128.

12. Bustamante, C.; Chemla, Y.R.; Forde, Y.R.; Izhaky, D. Annu. Mechanical Processes in Biochemistry. *Annu. Rev. Biochem.* **2004.** 73: 705-748.

13. Rohrbach, A.; Tischer, C.; Neumayer, D.; Ernst-Ludwig Florin, E.; Stelzer, H.K. Trapping and tracking a local photonic force microscope. *Rev. Sci. Instru.* **2004**. *75*: 2197.

14. Sheth, S.R.; Leckband, D. Measurements of Attractive Forces between Proteins and End-Grafted Poly(Ethylene Glycol) Chains. *PNAS*. **1997**, *94*(16): 8399-8404.

15. Schuster, S.C.; Swanson, R.V.; Alex, L.A.; Bourret, R.B.; and Simon, M.I. Assembly and Function of a quaternary signal transduction complex monitored by surface plasmon resonance. *Nature* **1993**. *36*: 343-347.

16. Wertz, C.F. and Santore, M.M. Adsorption and Relaxation Kinetics of Albumin and Fibrogen on Hydrophobic Surfaces: Single-Species and Competitive Behavior. *Langmuir* **1999**. *15* (26): 8884-8894.

17. Schuck, P. Use of Surface Plasmon Resonance to Probe the Equilibrium and Dynamic Aspects of Interactions Between Biological Macromolecules. *Annu. Rev. Biophys. Biomol. Struct.* **1997**. *26*: 541-566.

18. Shumaker-Parry, J.S.; Campbell, C.T. Quantitaive Methods for Spatially Resolved Adsorption/Desorption Measurements in Real Time by Surface Plasmon Resonance Microscopy. *Analytical Chemistry*. **2004**, *76*(4): 907-917.

19. Liebert, R.B.; Prieve, D.C. Species-specific long range interactions between receptor/ligand pairs. *Biophysical Journal*. **1995**, *66*(1): 66-73.

20. Robertson, S. K. and Bike, S. G. Quantifying Cell-Surface Interactions Using Model Cells and Total Interal Reflection Microscopy. *Langmuir* **1998**. *14*(4):928-934.

21. Robertson, S.K.; Uhrick, A.F.; Bike, S.G. TIRM Measurements with Cells and Liposomes. *J. Colloid Interface Sci.* **1998**, *202*(1):208-211.

22. Singh-Zocchi, M.; Dixit, S.; Ivanov, V.; Zocchi, G. Single-Molecule Detection of DNA Hybridization. *PNAS*. **2003**, *100*(13): 7605-7610.

23. Leckband, D.; Israelachvili, J. Intermolecular forces in biology. *Q. Rev. of Biophys*. **2001**, *34*(2):105-267.

24. Kim H, Park JH, Cho IH, Kim SK, Paek SH and Lee H. Selective immobilization of proteins on gold dot arrays and characterization using chemical force microscopy. *Journal of Colloid and Interface Science*. **2009**, *334*(2):161-166.

25. Costa LT, Vilani C, Peripolli S, Stavale F, Legnani C and Achete CA. Direct immobilization of avidin protein on AFM tip functionalized by acrylic acid vapor at RF plasma. *Journal of Molecular Recognition*. **2012**, *25*(5):256-261.

26. Ducker, W.A.; Senden, T.J.; Pashley, R.M. Direct Measurement of colloidal forces using an atomic force microscop. *Nature*. **1991**, 353(6341):239-241.

27. Mirsaidov, U.; Scrimgeour, J.; Timp, W.; Beck, K.; Mir, M.; Matsudaira, P.; Timp, G. Live cell lithography: using optical tweezers to create synthetic tissue. *Lab on a chip* **2008,** *8*:2174-81.

28. Murai, T.; Hokonohara, H.; Takagi, A.; Kawai, T. Atomic Force Microscopy Imaging of Supramolecular Organization of Hyaluronan and Its Receptor CD44. *Physical Review Letters* **2005,** *94:*94-97.

29. Everett, W,M. "Evanescent Wave and Video Microscopy Methods for Directly Measuring Interactions between Surface-Immobilized Biomolecules." Order No. 3281053 Texas A&M University, **2007**. Ann Arbor: *Proquest*.

30. Schurr, J.M. Dynamic light scattering of biopolymers and biocolloids. *CRC critical reviews in biochemistry* **1977,** *4*:371-431.

31. Dubacheva G.V.; Curk, T.; Auzely-Velty, R.; Frenkel, D.; Richter, R.P. Designing Multivalent probes for tunable superselective targeting. *PNAS*. **2015**. *112*(18): 5579-5584.

32. Wang, Y.; Gildersleeve, J. C.; Basu, A.; Zimmt, M. B. Photo- and biophysical studies of lectin-conjugated fluorescent nanoparticles: reduced sensitivity in high density assays. *The journal of physical chemistry. B* **2010,** *114*:14487-94.

33. Smith, E.A.; Thomas, W.D.; Kiessling, L.L.; Corn, R.M. Surface plasmon resonance imaging studies of protein-carbohydrate interactions. *Journal of the American Chemical Society* **2003,** *125*:6140-8.

34. Wang, W.; Wang, S.; Liu, Q.; Wu, J.; Tao, N. Mapping single-cell-substrate interactions by surface plasmon resonance microscopy. *Langmuir : the ACS journal of surfaces and colloids* **2012,** *28*:13373-9.

35. Lisse, D.; Richter, C.P.; Drees, C.; Birkholz, O.; You, C.; Rampazzo, E.; Piehler, J. Monofunctional stealth nanoparticle for unbiased single molecule tracking inside living cells. *Nano Lett* **2014,** *14* (4):2189-95.

36. Guo, S.-M.; Bag, N.; Mishra, A.; Wohland, T.; Bathe, M. Bayesian Total Internal Reflection Fluorescence Correlation Spectroscopy Reveals hIAPP-Induced Plasma Membrane Domain Organization in Live Cells. *Biophysical journal* **2014,** *106*:190-200.

37. Banerji, S.; Wright, A.J.; Noble, M.; Mahoney, D.J.; Campbell, I.D.; Day, A.J.; Jackson, D.G. Sturctures of the Cd44-hyaluronan complex provide insight into a fundamental carbohydrate-protein interaction. *Nature: struc. & mol. bio* **2007**, *14*:234-239.

38. Aspee, A.; Lissi, E. Interfacial Free Energy of Alkanols in Aqueous Solutions: Dependence with Hydrophobicity and Topology of the Solute. *J. Colloids Interf. Sci.* **1996**, *179*(1):298-302.

39. Eichmann, S.L.; Meric, G.; Swavola, J.C.; Bevan, M.A. Diffusing Colloidal Probes of Protein Carbohydrate Interactions. *Langmuir*, **2013**, *29*:2299-2301.

40. Everett, W.N.; Wu, H.; Anekal, S. G.; Sue, H..; Bevan, M.A. Diffusing Colloidal Probes of Protein and Synthetic Macromolecule Interactions. *Biophysical Journal* **2007,** *92*:1005-1013.

41. Everett, W.N.; Bevan, M.A. kT-Scale interactions between supported lipid bilayers. *Soft Matter* **2014,** *10*:332.

42. Bevan, M.A.; Prieve, D.C. Direct Measurement of Retarded van der Waals Attraction. *Langmuir*. **1999**. *15*:7925-7936.

43. Prieve, D. C.; Russel, W. B. Simplified Predictions of Hamaker Constants from Lifshitz Theory. *J. Colloid Interface Sci.* **1988,** *125*:1.

44. J. Mahanty and B. W. Ninham. *Dispersion Forces*. New York: Academic Press, 1976. Book.

45. Milner, S. T. Polymer Brushes. *Science* **1991,** *251*(4996): 905-914.

46. Prieve, Dennis C., and Nasser A. Frej. Total internal reflection microscopy: a quantitative tool for the measurement of colloidal forces. *Langmuir*. **1990**, *6*(2): 396-403.

47. Eichmann, S.L.; Anekal, S.G.; Bevan, M.A. Electrostatically Confined Nanoparticles Interactions and Dynamics. *Langmuir*, **2008**, *24*:714-721.

48. Eichmann, S.L.; Bevan, M.A. Direct measurements of protein stabilized gold nanoparticle interactions. *Langmuir*, **2010**, *26*:14409-14413.

49. Beckham, R.E. “Confocal Microscopy Study of Colloidal Sedimentation and Crystallization.” Order No. 3321640 Texas A&M University, **2008**. Ann Arbor: *ProQuest*.

50. Duncan, G.A. “Diffusing Colloidal Probes of Biospecific Interactions and Biological Interfaces.” Johns Hopkins University, **2014**.

51. Sackman, E. Supported Membranes: Scientific and Practical Applications. *Science*. **1996**, *271*(5425):43-48.

52. Tanaka, M.; Sackman, E. Polymer-supported membranes as models of the cell surface. *Nature*. **2005**, *437*(7059):656-663.

53. Felgner, J.H.; Kumar, R.; Sridhar, C.N.; Wheeler, C.J.; Tsai, Y.J.; Border, R.; Ramsey, R.; Martin, M.; Felgner, P.L. Enhanced gene delivery and mechanism studies with a novel series of cationic lipid formulations. *Journal of Biological Chemistry*. **1994**, *269*(4):2550-2561.

54. Macdonald, R.C.; Macdonald, R.I.; Menco, B.P.M.; Takeshita, K.; Subbarao, N.K.; Hu, L.R. Biochimica Et Biophysica Acta **1061** (2), 297 (1991).

55. Agus, D.B.; Alexander, J.F.; Arap, W.; Ashili, S.; Aslan, J.E.; Austin, R.H.; Backman, V.; Bethel, K.J.; Bonneau, R.; Chen, WC.; Chen-Tanyolac, C.; Choi, N. C.; Curley, S.A.; Dallas, M.; Damania, D.; Davies, P.C.W.; Decuzzi, P.; Dickinson, L.; Estevez-Salmeron, L.; Estrella, V.; Ferrari, M.; Fischbach, C.; Foo, J.; Fraley, S.I.; Frantz, C.; Fuhrmann, A.; Gascard, P.; Gatenby, R.A.; Geng, Y.; Gerecht, S.; Gillies, R.J.; Godin, B.; Grady, W.M.; Greenfield, A.; Hemphill, C.; Hempstead, B.L.; Hielscher, A.; Hillis, W.D.; Holland, E.C.; Ibrahim-Hashim, A.; Jacks, T.; Johnson, R. H.; Joo, A.; Katz, J.E.; Kelbauskas, L.; Kesselman, C.; King, M.R.; Konstantopoulos, K.; Kraning-Rush, C.M.; Kuhn, P.; Kung, K.; Kwee, B.; Lakins, J.N.; Lambert, G.; Liao, D.; Licht, J.D.; Liphardt, J.T.; Liu, L.; Lloyd, M.C.; Lyubimova, A.; Mallick, P.; Marko, J.; McCarty, O.J.T.; Meldrum, D.R.; Michor, F.; Mumenthaler, S.M.; Nandakumar, V.; O'Halloran, T.V.; Oh, S.; Pasqualini, R.; Paszek, M.J.; Philips, K.G.; Poultney, C.S.; Rana, K.; Reinhart-King, C.A.; Ros, R.; Semenza, G.L.; Senechal, P.; Shuler, M.L.; Srinivasan, S.; Staunton, J.R.; Stypula, Y.; Subramanian, H.; Tlsty, T.D.; Tormoen, G.W.; Tseng, Y.; van Oudenaarden, A.; Verbridge, S. S.; Wan, J.C.; Weaver, V.M.; Widom, J.; Will, C.; Wirtz, D.; Wojtkowiak, J.; Wu, P.H. A physical sciences network characterization of non-tumorigenic and metastatic cells. *Scientific reports* **2013,** *3*: 1449.

56. Zöller, M. CD44: Can a cancer-initiating cell profit from an abundantly expressed molecule? *Nature Reviews, Cancer*. **2011**, *11*:254-267.

57. Raman, P.S.; Alves, C.S.; Wirtz, D.; Konstantopoulos, K. Dynamic Kinetic and Molecular Requirements Govern CD44 Binding to Hyaluronan versus Fibrin(ogen). *Biophysical Journal*. **2012**, *103*:415-423.

58. Dubacheva, G.M.; Curk, T.; Auzely-Velty, R.; Frenkel, D.; Ritcher, R.P. Designing multivalent probes for superselective tunable targeting. *PNAS*. **2015**, *112*(18):5579-5584.

59. Naor D, Sionov RV, Ish-Shalom D.. CD44: structure, function, and association with the malignant process. *Adv Cancer Res*. **1997**, *71*:241–319.

60. Heldin, P.; Karousou, E.; Bernert, B.; Porsch, H.; Nishitsuka, K.; Skandalis S.S. Importance of hyaluronan-CD44 interactions in inflammation and tumorigenesis. *Connect Tissue Res*. **2008**, *49*:215–8

61. Jordan, Andre R. et al. The Role of CD44 in Disease Pathophysiology and Targeted Treatment. *Frontiers in Immunology*. **2015**, *6*:182

62. Anand, M.T.; Kumar, S. CD44:A Key Player in Breast Cancer. *Indian Journal of Cancer*. **2014**, *51*(3):247-249.

63. Olczyk, P.; Komosinska-Vassev, K.; Winsz-Szczotka, K.; Kuznik-Trocha, K.; Olczyk, K. Hyaluronan: structure, metabolism, functions, and role in wound healing. *Postepy Hig Med Dosw*. **2008**, *62*:651–659.

64. Collis, L.; Hall, C.; Lange, L.; Ziebell, M.; Prestwich, R.; Turley, E.A. Rapid hyaluronan uptake is associated with enhanced motility: implications for an intracellular mode of action. *FEBS Lett*. **1998**, *440*:444–449.

65. Misra, Suniti et al. Interactions between Hyaluronan and Its Receptors (CD44, RHAMM) Regulate the Activities of Inflammation and Cancer. *Frontiers in Immunology* **2015**, *6*: 201.

66. Chan, Y-H.M.; Boxer, S.G. Model membrane systems and their applications. *Current Opinion in Chemical Biology*. **2007**, *11*:1-7.

67. Koenig, B.W.; Gawrisch, K.; Krueger, S.; Orts, W.; Majkrzak, C.F.; Berk, N.; Silverton, J.V. Neutron reflectivity studies of single lipid bilayers supported on planar substrates. Basic Life Sciences. 1996, 64:205-213.

68. Thompson, N. L.; Pearce, K. H.; Hsieh, H. V. Total internal reflection fluorescence microscopy: application to substrate-supported planar membranes. *Eur. Biophys. J. Biophy.***1993**, *22*(5):367–378.

69. Yang, T.; Baryshnikova, O. K.; Mao, H. B.; Holden, M. A.; Cremer, P. S. Investigations of Bivalent Antibody Binding on Fluid-Supported Phospholipid Membranes: The Effect of Hapten Density. *J. Am. Chem. Soc.* **2003**, *125*(16):4779–4784.

70. Diaz, A.J.; Albertorio, F.; Daniel, S.; Cremer, P.S. Double Cushions Preserve Transmembrane Protein Mobility in Supported Bilayer Systems. *Langmuir*. **2008**, *24*(13):6820-6826.

71. Bevan, M.A.; Prieve, D.C. Forces and Hydrodynamic Interactions between polystyrene surfaces with absorbed PEO-PPO-PEO. **2000**, *16*:9274-9281.

72. van Meer, G.; Voelker, D.R.; Feeigenson, G.W. Membrane lipids: where they are and how they behave. *Nature Rev. Mol. Cell Biol.* **2008**, *9*:112-124.

73. van Meer, G.; de Kroon, A.L.P.M. Lipid map of the mammalian cell. *J Cell Science*. **2011**, *124*:5-8.

74. Lee, A. Membrane structure. *Current Biology*. **2011**, *11*(20):R811-R814.

75. Simmons, K.; Iknonen, E. Functional rafts in cell membranes. *Nature*. **1997**, *387*: 569-572 .

76. Minn, A.J.; Gupta, G.P.; Siegel, P.M.; Bos, P.D.; Shu, W.; Giri, D.D.; Viale, A.; Olshen, A.B.; Gerald, W.L.; Massague, J. **Genes that mediate breast cancer metastasis to lung.** *Nature* **2005**, ***436*:**518-524.

77. Sheridan, C.; Kishimoto, H.; Fuchs, R.K.; Mehrota, S.; Bhat-Nakshatri, P.; Turner, C.H.; Goulet, R.; Badve, S.; Nakshatri, H. $CD44^{+}/CD24^{-}$ breast cancer cells exhibit enhanced invasive properties: an early step necessary for metastasis. *Breast Cancer Research*. **2006**, *8*:R59.

78. Wirtz, D.; Konstantopoulos, K.; Searson, P.C. The physics of cancer: the role of physical interactions and mechanical forces in metastasis. *Nature Rev. Cancer*. **2011**, *11*:512-522.

79. Lee-Sayer, S.S.M.; Dong, Y.; Arif, A.A.; Olsson, M. Brown, K.L.; Johnson, P. The where, when, how, and why of hyaluronan binding by immune cells. *Frontiers in Immunology*. **2015**, *6*(150):1-12.

80. Jones, M.N. Surfactants in membrane solubilisation. *Int. J. of Pharmacuetics*. **1999**, 177:137-159.

8 VITA

Name:	Samantha Mercedes Brandon
Address:	Samantha M Brandon may be contacted through Dr. M. A. Bevan at the Chemical & Biomolecular Engineering Department, Johns Hopkins University, Baltimore, MD 21218
Email Address:	smbrandon3@gmail.com
Education:	B.S. Chemical & Biomolecular Engineering, Johns Hopkins University, 2014, Baltimore, MD